September 19, 2017

MASTER'S THESIS

TOWARDS MRI-GUIDED RADIATION THERAPY OF REGIONAL LYMPH NODES IN BREAST CANCER PATIENTS

M.L. Groot Koerkamp

Faculty of Science and Technology
Technical Medicine

Exam committee:

Prof. Dr. D.G. Norris
Dr. H.J.G.D van den Bongard
Dr. ir. F.F.J. Simonis
Drs. A.G. Lovink
Dr. ir. M.E.P. Philippens
E. Groot Jebbink, MSc

UMC Utrecht

UNIVERSITY OF TWENTE.

Examination committee

Chairman	Prof. dr. D.G. Norris *Faculty of Science and Technology, University of Twente*
Medical supervisor	Dr. H.J.G.D. van den Bongard *Department of Radiotherapy, UMC Utrecht*
Technical supervisor University of Twente	Dr. ir. F.F.J. Simonis *Faculty of Science and Technology, University of Twente*
Process supervisor	Drs. A.G. Lovink *Department of Technical Medicine, University of Twente*
External member	E. Groot Jebbink, MSc *Department of Technical Medicine, University of Twente*
Technical supervisor UMC Utrecht	Dr. ir. M.E.P. Philippens *Department of Radiotherapy, UMC Utrecht*

Additional supervisors

Technical supervisor UMC Utrecht	Dr. A.C. Houweling *Department of Radiotherapy, UMC Utrecht*
Medical supervisor *6 week clinical internship*	Drs. C.E. Kleynen *Department of Radiotherapy, UMC Utrecht*

Acknowledgements

In this Master's thesis, I proudly present to you the final result of my graduation project for the Medical Imaging and Interventions track of the Technical Medicine master. For the last 46 weeks, I have been working at the Department of Radiotherapy of the UMC Utrecht. Here I got the chance to develop myself in a lot of different aspects and to collaborate with people in a lot of different disciplines. Although this is not a PhD thesis, and therefore, according to some of my supervisors, no acknowledgements should be included, I would still like to add them as the opportunity to thank some people.

First of all, I would like to thank Desiree and Marielle for giving me the opportunity of doing my graduation project on this department without having any experience with other Technical Medicine students. I am grateful for all possibilities, flexibility and support that you provided during this internship. Desiree, thank you as well for your supervision in my clinical activities, for sharing your extensive knowledge, and for always being available to answer any of my questions. Marielle, thank you for all your explanation on MRI topics, the practical MRI lessons and your input for my technical approach in the different topics of this research. I would also like to thank Anette for her input, for the helpful feedback on my thesis and her enthusiasm when brainstorming about my ideas. Furthermore, I would like to thank Stephanie de Waard for the help in the LN identifaction on MRI and Karin Kleynen for the supervision of the 6-week clinical internship at the start of my graduation internship.

Frank, although I did not see you very frequently, I always enjoyed our meetings. Even though the contacts sometimes were mostly an update from my side without specific questions, you were always critical and helpful to make me think about the (clinical) relevance of my ideas. In addition, you helped me in thinking about the boundaries I had to keep in mind for this project. Annelies, thank you for being my process supervisor. I have learned and experienced a lot during my interships the last two years. The intervision and the conversations at the end of each internship really helped me to reflect on it.

A special thank you is addressed to Tristan and Ramona, who helped me finding my way in this project and in coordinating a patient study. I would also like to thank Madelijn, for her help in contact with study patients and practical study issues. For instance the MRI orders, which Jeanine also helped me with. Tuan and Ellart, thank you for all the help and explanation during MRI scanning of volunteers and study patients. In addition, I want to thank the (PhD) students of the department for the pleasant distraction during lunch and table football breaks. I would also like to thank all my friends for the reflection times during coffee breaks or drinks at D.R.V. Euros and for sharing their room or house for my overnight stays in Enschede and Utrecht.

Special thanks also goes to my parents, Jos and Alien. You have always encouraged me to make my own choices. I am especially grateful for your support and help when I decided about my study switch. Thank you for your support in every possible way. My sister Iris, in some things you are way ahead of me. You show me that it is important to do what you like and makes you happy. Thank you for this and keep on doing this. Nick, the last couple of years you showed me your enormous perseverance in following and completing your own Master's. I admire how you did that and it helped me in completing mine. Thank you for being here, patiently listening to me and for helping me to put things into the real (instead of my imaginary) perspective.

Maureen Groot Koerkamp
7 September 2017

Contents

Abbreviations

2D	two dimensional
3D	three dimensional
ALND	axillary lymph node dissection
AxRT	axillary radiation therapy
bSSFP	balanced steady state free precession
CBCT	cone beam computed tomography
CoG	centre of gravity
CT	computed tomography
CTV	clinical target volume
DIR	deformable image registration
ELPS	external laser positioning system
ERE	electron return effect
FFE	fast field echo
FOV	field of view
GTV	gross tumour volume
ICV	infraclavicular
IGRT	image guided radiation therapy
IMRT	intensity modulated radiation therapy
LN	lymph node
MR	magnetic resonance
MRI	magnetic resonance imaging
OAR	organ at risk
PET	positron emission tomography
PTV	planning target volume
RT	radiation therapy
SCV	supraclavicular
SD	standard deviation
SN	sentinel lymph node
SNB	sentinel node biopsy
SSFP	steady state free precession
SSIM	structural similarity measure
TAS	thorax arm support
TFE	turbo field echo
TSE	turbo spin echo
UMC	University Medical Center
VMAT	volumetric modulated arc therapy
WBI	whole breast irradiation

List of figures & tables

Abstract

Regional radiation therapy (RT) for breast cancer patients with a tumour-positive sentinel node biopsy is increasingly preferred over axillary lymph node dissection. Regional RT shows less arm morbidity, but is still associated with lymphoedema and impaired shoulder function. Currently, computed tomography (CT) scans are used for RT treatment preparation. However, recently magnetic resonance imaging (MRI) sequences were developed for individual lymph node (LN) visualization in RT treatment position. The addition of MRI to the workflow of regional RT potentially leads to improved target definition. Furthermore, the MRI linac at the UMC Utrecht provides the possibility of daily MR imaging before and during treatment. This enables perfect online plan adaptation and intrafraction image guidance which may enable margin reduction. Therefore, the use of MRI in the regional RT workflow could improve normal tissue sparing and reduce treatment-induced toxicity. In this thesis several subjects relevant for MRI-guided radiation therapy of regional lymph nodes in breast cancer patients were explored.

MRI scans of five breast cancer patients (cTis-1bN0) participating in the TIMBRE patient study were acquired before start of any treatment. For each patient the scans consisted of: two to three 3D T_1-weighted turbo field echo scans (T1) with mDIXON reconstruction, one T_2-weighted turbo spin echo mDIXON and a coronal-sagittal interleaved cine MRI. Also sagittal cine MRIs of seven healthy volunteers were available.

*Inter*fraction displacement of individual LNs was measured on repeated T1 scans of the same patient. Scans were rigidly registered using two local boxes. Differences in LN center of gravity (CoG) position were determined. 127 LNs were identified. Displacements ranging from 1.55-2.47mm were found for different anatomical LN levels. These differed between the registration boxes. LNs moved independently from each other. The displacements were small, but are relevant for workflow development for individual LN irradiation, especially for hypofractionated stereotactic treatment. Very local verification of target position is important.
Furthermore, *intra*fraction motion of individual LNs was studied using the cine MRIs. An optical flow algorithm was used to pixel-wise register the cine slices to each other. The mean displacement vector of the LN pixels was calculated to get displacement with respect to the reference frame. Maximum peak-to-peak amplitude was determined. Average maximum displacements in left-right, superior-inferior and anterior-posterior direction ranged from 1.6-2.1mm. LN displacement was caused mainly by breathing motion, but some small baseline drifts were seen. The intrafraction displacements have to be taken into account when targeting individual LNs.

Another subject that was investigated is intrapatient contour propagation of LN delineations. It can be used for recontouring of a daily MRI before treatment for online plan adaptation on the MRI linac. Deformable image registration with the commercial software package ADMIRE Research (version 1.13.3, Elekta AB, Stockholm, Sweden) was tested. Mean distance between propagated and manual LN contours was 0.70mm with a standard deviation (SD) of 0.30mm. Average distance between the CoGs was 1.09mm (SD 0.60mm). The median propagated LN volume was 11% smaller than the manual volume. Overall distances were small, therefore, contour propagation is a good start for recontouring on a new scan. However, geometrical correctness and volumes of the contours have to be checked.

Lastly, the patient experiences during MRI scanning were evaluated. This was done with a short evaluation form after scanning. No severe painful, uncomfortable or anxious experiences were reported. Overall, the patients indicated that they could endure the scanning well. However, 4 out of 5 patients reported a type of physical complaint (e.g. sensitive back muscles or arm numbness) that was related to maintaining the same position for the duration of the scan set, which was up to 35 minutes.

In conclusion, the subjects that have been investigated are important for workflow development of MRI-guided RT of individual regional LNs. The results are valuable for workflow development for the MRI linac as well as for the addition of MRI to the current CT-based workflow. In the end, an MRI-guided approach will improve LN targeting accuracy and will lead to improved normal tissue sparing, thereby reducing treatment-induced toxicity and morbidity.

1 General introduction

1.1 Breast cancer

Breast cancer is the most common cancer in women in the Netherlands. In 2016, 14,511 women were diagnosed with breast cancer and 2,667 women with carcinoma in situ.[1] The lifetime risk for a Dutch woman for being diagnosed with breast cancer is 12-13%.[2] In 2006, it was found that the mortality of women between 55 and 74 years old was 24.3% lower than in 1986-1988, before the national breast cancer screening was introduced.[3] In addition, the screening program contributed to detection of breast malignancies in an earlier stage of the disease,[3] which is favourable for treatment options and prognosis.

1.1.1 Breast cancer treatment

Surgery is an important part of local treatment of breast cancer: this can be either breast-conserving surgery or removal of the whole breast, called mastectomy. After breast-conserving surgery, whole breast radiation therapy (RT) is indicated. After mastectomy chest wall irradiation is indicated for high-risk patients only. Whole breast and chest wall irradiation are given to increase local control and overall survival. In addition, (neo)adjuvant systemic therapy (i.e., cytotoxic chemotherapy, endocrine therapy or immunotherapy) is used to treat micrometastases.[3] Sentinel node biopsy (SNB) is currently the preferred method for lymph node staging in clinically node negative patients with T1/T2-breast carcinoma (cT1-2N0),[2,3] and can also be used for larger tumours.[4] It is performed in cN0 patients and also in patients with limited positive lymph nodes who are treated with neoadjuvant systemic therapy. More than 75% of lymph drainage from the breast is via the axillary lymph nodes (LNs).[3] The sentinel lymph node (SN) is usually located in the level I lymph nodes (lateral to the m. pectoralis minor) in the axilla (Figure 1.1).[5]

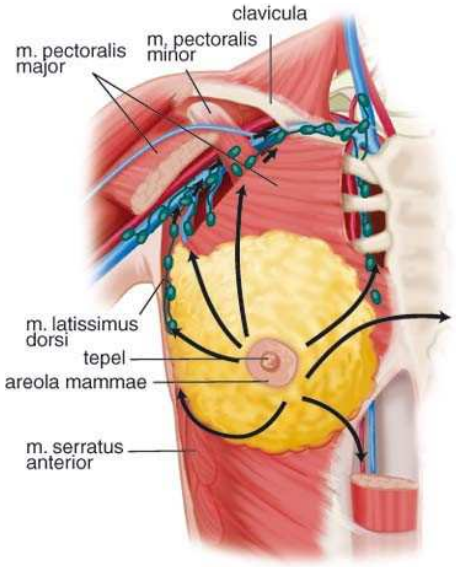

Figure 1.1: ***Lymph drainage system of the breast.***
Obtained from: De Jongh, et al., Fysische diagnostiek (2010)[6]

In case of a tumour-positive SN, axillary lymph node dissection (ALND) has long been the standard choice of treatment.[2,3] However, ALND is associated with arm morbidity, including lymph oedema, restriction in shoulder mobility, numbness, and paresthesias.[7–10] Recently, several clinical trials (including The American College of Surgeons Oncology Group (ACOSOG) Z0011 Randomized Trial,[11] and the International Breast Cancer Study Group (IBCSG) 23-01 multicentre randomised controlled trial[12]) have suggested that ALND might be overtreatment and could be omitted in selected patients group (e.g., with limited macrometastatic SN involvement[11] or micrometastatic SNs[12]). In addition, the AMAROS trial[13] showed that axillary RT (including the periclavicular region) provides comparable axillary control to ALND with significantly less arm morbidity. Clinical signs of lymph oedema were seen in 23% of the ALND patients versus 11% in the axillary RT group at 5 years follow-up.[13] Galimberti et al.[12] concluded that with current adjuvant systemic therapy further axillary dissection is unnecessary with SN micrometastases ($\leq$2 mm).[12] Referring to the AMAROS trial[13] Bundred et al.[14] stated that regional axillary RT and ALND for the treatment of macrometastases (>2 mm) are equivalent in their prevention of regional recurrence, but that regional RT is associated with less arm morbidity.[13,14]

1.1.2 Regional radiation therapy

Following the results from these trials,[11–13] regional RT is increasingly preferred as axillary treatment over ALND in patients with limited tumour-positive SNs. In addition, also patients with clinically tumour-positive LNs (N+) that become tumour-negative (N0) after neoadjuvant chemotherapy are eligible for regional RT instead of ALND. Regional RT in breast cancer patients is given to the axillary LN levels and can include the lower axilla, periclavicular and internal mammary LN areas. In the NCIC Clinical Trials Group MA.20 trial[15] and the EORTC 22922/10925 randomized, multicentre, phase 3 trial[16] reduced rates of breast cancer recurrence were found after RT to internal mammary and periclavicular LN areas in node-positive or high-risk node negative breast cancer patients. In current clinical practice, the use of RT to internal mammary LNs can vary. It is mostly given only in case of a tumour-positive internal mammary SN or a tumour-positive internal mammary LN on diagnostic imaging. Some institutes irradiate the internal mammary LNs also in patients with a medially or centrally located tumour and tumour-positive axillary lymph nodes. RT to the periclavicular LNs is given to high-risk patients, based on primary tumour characteristics and extensiveness of LN involvement.

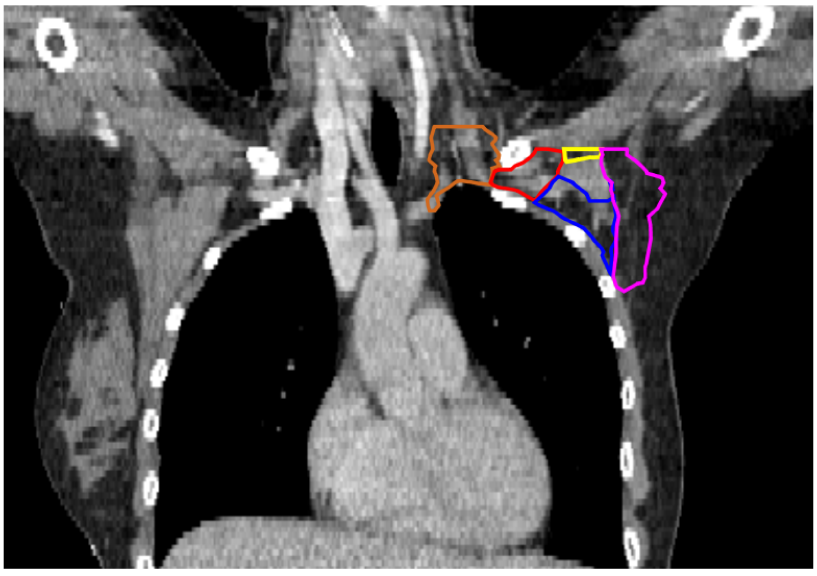

Figure 1.2: ***Example of LN level delineations on CT according to consensus guidelines.***
In pink: level 1, blue: level 2, yellow: level 2 (interpectoral region), red: level 3, and orange: level 4.

1.2 Current workflow for regional lymph node irradiation

Currently, target volume and organ at risk (OAR) delineation for regional RT planning is performed on computed tomography (CT) scans. Lymph node areas are contoured according to consensus guidelines[17] (Figure 1.2) using anatomical structures like vessels or muscles as reference, because individual lymph nodes are not clearly visible on CT. These lymph node levels are the clinical target volume (CTV) for regional RT. Additional margins are added to expand the target volume to account for variations in patient positioning and breathing motion during treatment. This produces the planning target volume (PTV). This results in relatively large RT targets, and therefore relatively high dose to surrounding normal tissues, including muscles, brachial plexus, lungs, and heart. Although axillary RT shows less morbidity than ALND, it has been associated with lymph oedema, radiation pneumonitis, and impaired shoulder function.[13,18,19] If target volumes can be defined more accurately, the radiated volume of normal tissue potentially decreases, possibly reducing treatment-induced toxicity and morbidity.

1.2.1 RT treatment plan

In preparation before the actual irradiation, the CT scan with all delineated structures is used to calculate the dose for a RT treatment plan. In most cases the same plan will be used for all treatment fractions. Before each treatment fraction on the conventional linear accelerator (linac), the patient is positioned using small tattoo points put on the skin to align with the isocentre of the linac shown by fixed laser lines. At several fractions, cone beam CT (CBCT) is used to verify patient position before RT delivery. An overview of the workflow is shown in Figure 1.3.

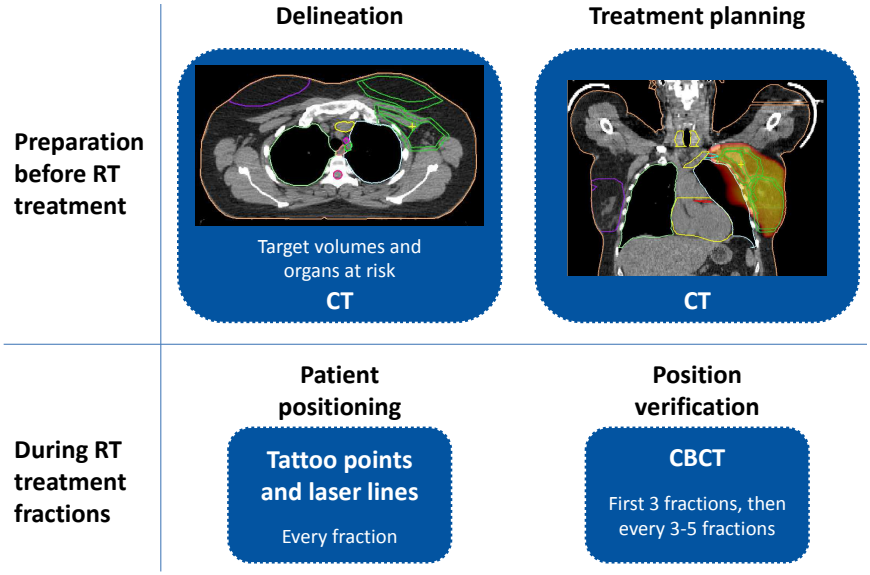

Figure 1.3: *Current conventional CT-based workflow for regional RT.*

1.3 Technological developments and recent studies

Technological developments in radiation hardware facilitate delivering radiation with increasing geometrical and dosimetric accuracy. Improvements in image guidance facilitate target volume definition before treatment as well as position verification during treatment, introducing the so called image guided radiation therapy (IGRT). These advances allow for dose escalation to the tumour,

without increasing radiation-induced toxicity to surrounding normal tissue. However, because conformation of the radiation field gets more accurate, all steps in the RT treatment and treatment preparation have to become more accurate. These include delineation of the target volumes and OARs, and verification of the position of the target volume. Therefore, imaging and image guidance during radiotherapy still become more and more important.[20]

1.3.1 The MRI linac

At the University Medical Center (UMC) Utrecht, a magnetic resonance imaging (MRI) linac system has been developed (Figure 1.4).[21,22] This system combines a diagnostic quality 1.5T MRI scanner (Philips, Best, the Netherlands) with a 7.2MV accelerator (Elekta AB, Stockholm, Sweden). It was shown that high quality images could be created while the radiation beam was on.[21] With this system, daily high-quality pre-treatment imaging becomes possible, as well as real-time MRI guidance during the irradiation. This will allow the use of the actual anatomical situation of the moment to correct for translations, rotations, and deformations.[22,23] Furthermore, MRI inherently has excellent soft tissue contrast compared to CT. Therefore, visualization of tumours and structures that cannot be visualized well on planning and cone beam CT will improve. Potentially, this combination of daily imaging and improved visualization of target structures leads to smaller treatment volumes. In addition, it will contribute to improving dose conformity. The dose to the target volume can be increased while the dose to normal tissue is reduced.[23] LNs are target volumes that are not clearly visualized on CT. Consequently, regional LN RT can potentially benefit from MRI guidance.

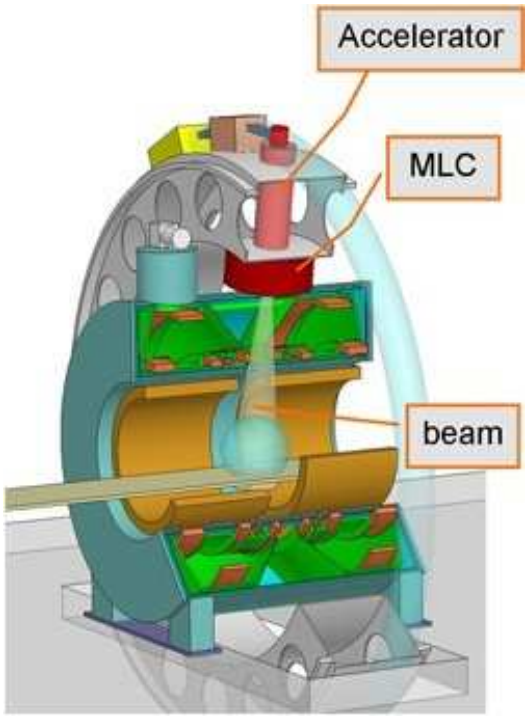

Figure 1.4: ***Schematic drawing of the MRI linac.*** *Obtained from: Lagendijk et al. (2016)*[23]
Abbreviation: MLC: multileaf collimator.

1.3.2 Individual LN visibility on MRI

Several studies have focused on MRI for LN imaging in the axilla.[24,25] These studies evaluated whether MRI could be used for detection or exclusion of axillary lymph node metastasis, to potentially replace SNB. Some protocols seemed promising for excluding axillary LN metastases.[24] However, since these techniques were primarily developed for diagnostic purposes, they were not optimized for regional RT planning. The primary purpose of scans for RT planning is accurate and

geometrical correct target definition, OAR delineation and dose planning. For breast cancer usually no contrast agents are administered. In addition, a flat table top is used to match patient positioning on the linac table during treatment. At the UMC Utrecht, a study[26] was performed in healthy volunteers to evaluate and optimize MRI sequences specially aimed at the use for RT treatment purposes in RT supine position. The possibility of individual LN delineation was assessed. Although no gold standard for the number of LNs was available, and LN identification rate could therefore not be verified, it was shown that it was feasible to identify individual axillary and supraclavicular LNs in supine RT position. Two T2-weighted sequences (T2-VISTA and T2-TSE) showed the highest number of LNs, and a T1-weighted fast field echo (FFE) showed the most anatomical information (Figure 1.5).[26] A combination of these scans could be a good set for individual LN delineation.

In a feasibility study,[27] it was evaluated whether individual LN identification with the MRI scans mentioned before[26] was also possible in breast cancer patients. In addition, LN detection rates were compared to the standard postoperative RT-planning CT. It was shown that all the individual LNs but one could be spatially correlated between the pre- and post-operative MRI sessions. LN detection rate on postoperative MRI was significantly higher than on CT (median number of LNs 25 and 11, for MRI and CT respectively). Furthermore, individual LN volumes delineated on MRI were compared to standard delineated axillary level volumes. Total LN volumes within an axillary level were at most 3% of the volume of the respective levels. These results show that use of MRI in RT treatment planning could lead to more accurate target delineation and potentially a reduction in RT target

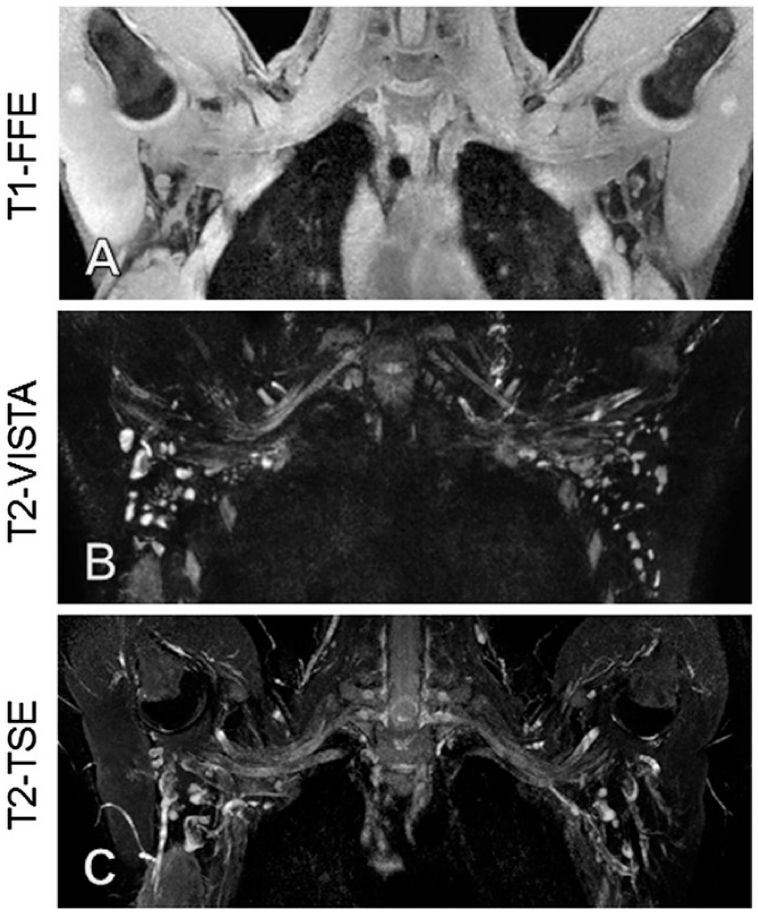

Figure 1.5: ***Coronal MRI slices showing individual axillary lymph nodes.*** *The different MRI sequences that are shown are: A: T1-weighted fast field echo (T1-FFE) showing clear anatomical information, and both B: T2-weighted (T2w) volumetric isotropic acquisition (T2-VISTA), and C: T2w turbo spin echo (T2-TSE) showing a high number of LNs. (Modified image from: Van Heijst et al.[26])*

volume, thereby sparing more normal tissue.[27] With online MRI guidance, which is possible with the MRI linac, accurate high dose delivery to individual LNs may be possible without the use of relatively large additional margins to account for uncertainty in target position.

1.3.3 Individual LN boosting

Currently, the treatment for tumour-positive LNs (after neoadjuvant chemotherapy) is surgery or a five to ten fractions RT boost to the involved lymph nodes additional to whole breast irradiation (WBI) and axillary RT (AxRT). Van Heijst et al.[28] explored axillary LN boosting on the MRI linac using a single dose ablative RT, sequentially to WBI and AxRT on a conventional linac. Because of possible increase in skin dose due to the electron return effect (ERE) in a 1.5T magnetic field,[29] WBI in combination with AxRT was planned on a conventional linac in absence of magnetic field. Sequential LN boosting plans were generated with specially developed MRI linac treatment planning software,[30] incorporating the 1.5T magnetic field effects (Figure 1.6). It was shown that individual LN boosting up to an ablative single RT dose was feasible for individual LNs in all axillary LN levels, including LNs close to OAR, such as chest wall, brachial plexus and spinal cord. All clinical constraints for OAR dose were met.[28] LN boosting might eventually serve as an alternative to ALND or conventionally fractionated RT in patients with tumour-positive LNs and decrease the risk of treatment-induced toxicity , which may increase quality of life compared to axillary surgery or standard regional RT.

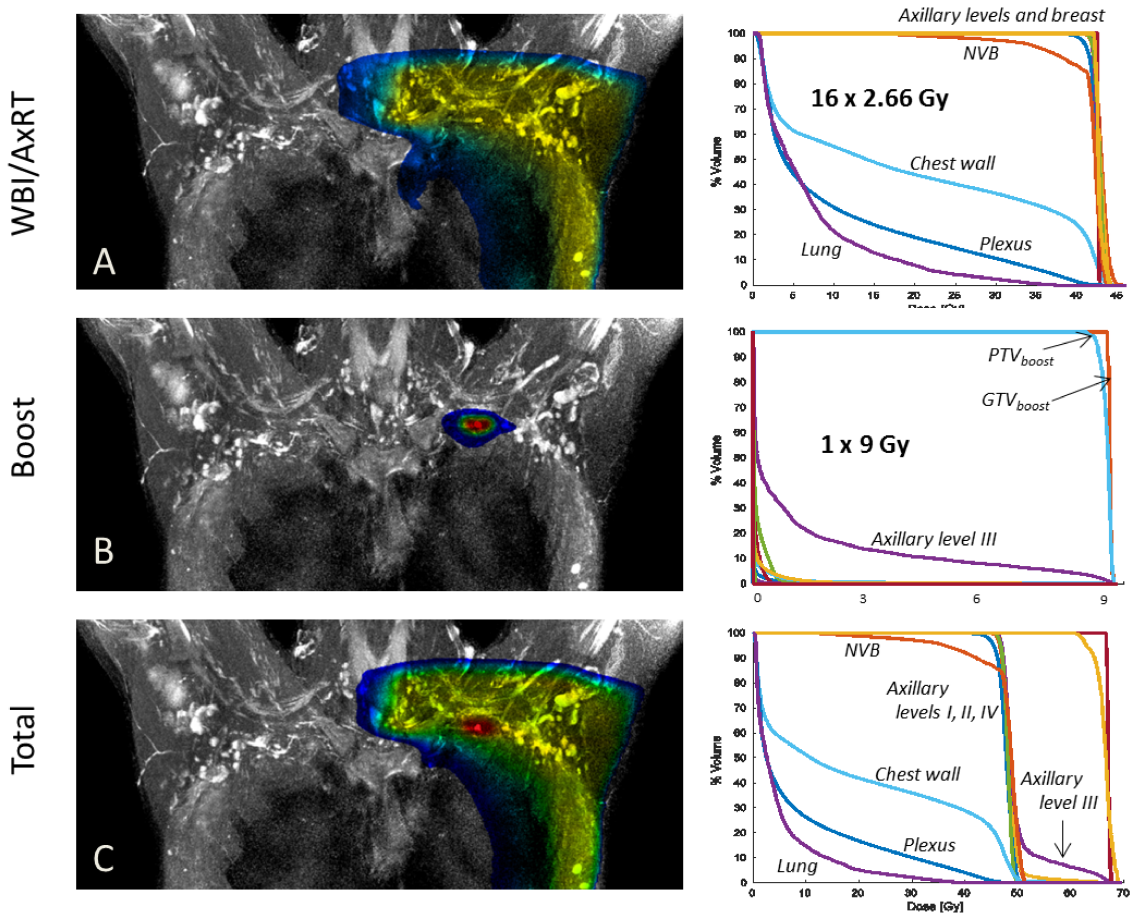

Figure 1.6: ***Example of a dose plan from Van Heijst et al.***[28] *The dose-volume histograms including OARs of the plans are shown on the right. In A) the WBI/AxRT plan for 16x 2.66 Gy is shown, in B) the individual LN boost of in this case 1x 9Gy. C) shows the addition of the two dose plans with the EQD_2 model. Excellent target coverage for the LN is achieved without exceeding the dose constraints for the OARs.*

1.4 MRI guidance for regional RT

With MRI-guided radiotherapy individual LNs can be visualized. This could enable RT delivery to individual LNs instead of whole axillary LN levels. Different approaches are possible. For instance, only tumour-positive LNs, the gross tumour volume (GTV), can be targeted. Furthermore, an adaptation of the CTV delineation for elective RT can be chosen. The axillary CTV levels can be adapted to smaller individual LN CTVs for LNs that are at risk for microscopic tumour spread.

In this thesis MRI guidance can refer to two different approaches:

- addition of MRI to the current CT-based workflow, or;
- the use of the MRI linac.

In the first approach the main improvement is the more accurate definition of target volumes when using MRI instead of or in addition to CT scans. By this the total LN CTV volume might be reduced, which will lead to better sparing of OARs. The position verification on the conventional linac will be the main limiting step in the accuracy since no online MR imaging will be available.
In the second approach, the target definition as well as the position verification accuracy will improve. With online MRI guidance and target verification, patient positioning accuracy and correction for daily positioning variations will improve compared to the current CT workflow which uses skin tattoos without daily imaging. This will enable the use of smaller CTV-PTV margins and facilitate dose escalation to the target, while it will result in better sparing of the normal surrounding tissue.

The primary goal of an MRI-guided approach for regional lymph node irradiation is to reduce treatment-induced toxicity, which could lead to increased quality of life. In the future, such a treatment could potentially replace current treatments, and become a safe and efficient, minimally invasive alternative to axillary surgery or conventionally long fractionated RT boost schedules for pathologically involved lymph nodes.

1.5 Aim of this thesis

Before we are able to make use of the aforementioned advantages of MRI guidance for regional lymph node irradiation, several subjects that are important for MRI-guided treatment planning and delivery have to be investigated. Therefore, the aim of this thesis was:

To explore MRI-guided radiation therapy of regional lymph nodes in breast cancer patients.

The different objectives that were evaluated for this aim were:

- Quantification of *inter*fraction axillary lymph node displacement
- Quantification of *intra*fraction axillary lymph node motion
- Exploration of intrapatient contour propagation for lymph node delineation
- Assessment of patient comfort and posture endurance during MRI scans

2 Study population and MRI data

2.1 Study population

2.1.1 TIMBRE patients

All patient data used in this study was acquired for the TIMBRE (*Towards implementation of online MRI-guided radiation therapy in breast cancer patients*) patient study[31] (NL56683.041.16) that is currently being performed at the radiotherapy department of the UMC Utrecht. The aim of the TIMBRE study is to develop an adaptive MRI-only workflow for local and regional lymph node irradiation for the MRI linac, in breast cancer patients.[31] Data of the first five patients (Table 2.1) who signed informed consent for this study and underwent MR scanning of the axillary region was used for analyses for this thesis. For all patients MR scanning was performed between diagnosis of the breast cancer and the start of treatment.

Inclusion criteria for eligibility were:[31]

- Female gender;
- Age $\geq$ 18 years old;
- cTis-4 N0-3 M0-1 breast cancer;
- Written informed consent provided.

Exclusion criteria were:[31]

- Legal incapacity;
- Presence of properties included in MRI exclusion criteria of the UMC Utrecht;
- Previously known inability to undergo the scanning procedure;
- Previous surgery of the ipsilateral axillary and/or supraclavicular region.

2.1.2 Healthy volunteers

In addition to data of five TIMBRE patients, also MR imaging data of seven healthy volunteers was available. Information about age and BMI is not available.

Table 2.1: *Patient characteristics of the TIMBRE study population.*

Study ID	Age [years]	BMI [kg/m^2]	Clinical TNM stage	Side	Biopsy pathology
01	64	29.2	cTisN0Mx	Left	DCIS grade 2
02	51	27.8	cTisN0Mx	Left	DCIS grade 2-3
03	68	29.1	cTisN0Mx	Left	Papillary carcinoma
04	49	22.5	cT1bN0Mx	Right	Carcinoma with medullary characteristics
05	56	24.9	Questionable benign*	Right	Adenomyoepithelioma*

Abbreviations: BMI = body mass index, T = tumour, N = nodal, M = metastasis
* DCIS was found with same biopsy pathology in contralateral breast

2.2 Data acquisition

The MR sequences that are used were previously optimized for individual lymph node imaging.[26,27] The MR imaging can be used to evaluate interfraction lymph node motion, patient positioning variations, and intrafraction lymph node motion. In addition, posture endurance and patient comfort can be evaluated. Eventually, results of the TIMBRE data can be used to develop a workflow for individual LN treatment on the MRI linac that is adapted to deal with lymph node displacement and the variations in patient positioning.

2.2.1 MRI scanning set-up

Between December 2016 and April 2017, the five TIMBRE patients were scanned on a 1.5 T wide bore MRI scanner (Philips Ingenia, Best, the Netherlands) at the radiotherapy department of the UMC Utrecht. Scanning was performed on a flat table top. Patients were positioned on 5°wedge and an MR compatible thorax-arm support (TAS) in supine position with arms in abduction (RT position). The anterior receive coil was placed upon height adjustable plastic coil bridges, such that the coil would not deform the outer body contour, see Figure 2.1. A posterior receive coil located in the scanner table was also used.

Figure 2.1: ***MRI scanning set-up with flat table top, TAS, coil bridges and receive coils.***

Volunteer data was acquired in April 2012 at a 1.5T MRI scanner (Philips Ingenia, Best, the Netherlands). Volunteers were also scanned in supine position with arms abduction. However, the exact patient set-up, patient support and positioning of the coils is unknown.

2.2.2 Repositioning

To simulate interfraction motion, or daily variations in patient positioning that can occur between two irradiation fractions, a couple of MRI sequences were repeated in each patient in the same session. The patient was asked to descend from the scanner table between the scanning blocks. For patient 01 and 04 an external laser positioning system (ELPS) in combination with skin tattoos was used for repositioning. For the other three patients no laser system and tattoo points were used. However, TAS position settings were left the same.

2.2.3 Sequence optimization

The patients that were used in this study were also used for further optimization of previously developed sequences in the TIMBRE study. Due to this, scanning protocols differed somewhat between the patients. After each patient, all scans were evaluated with a radiation oncologist (DvdB), an MR imaging physicist (MP), and a medical physicist (AH) to decide on image quality and necessity of sequence adaptation.

Table 2.2: *Imaging parameters of the MRI scans.*

Sequences: / Parameters:	T1 TFE	T2 TSE	cine (SSFP)*	cine (bSSFP)
TR/TE [ms]	5.4 / 2.0 / 3.8[a]	2651/70	2.9/1.39	2.5/1.04
Fat suppression	mDIXON	mDIXON		
Dimensionality	3D	2D	2D	2D
(In-plane) FOV	500 x 500 x 250 mm^3 / 500 x 500 x 350 mm^3 [b]	400 x 400 mm^2	500 x 500 mm^2	400 x 400 mm^2
Acquired resolution	1.25 x 1.25 x 1.25 mm^3	1.00 x 1.25 mm^2	2.01 x 2.00 mm^2	NA[d]
Slice thickness	-	3.0mm / 2.5 mm[c]	8mm	10mm
Reconstructed resolution	0.95 x 0.95 x 1.25 mm^3	0.62 x 0.62 mm^2	1.73 x 1.73 mm^2	1.04 x 1.04 mm^2
Scan time [min:s]	4:52	5:34	1:01 (total) 0.6 s (per slice)	1:01 (total) 0.3 s (per slice)

Abbreviations: FOV: field of view, TR: repetition time, TE: echo time, 3D: three dimensional, 2D: two dimensional, NA: not available.
* Interleaved acquisition order: subject 01: 'cor-sag' and subjects 02-05: 'cor-sag-sag-cor'.
[a] TR/TE1/TE2 (ms)
[b] 250mm for subject 01 and 02, 350mm for 03 05
[c] 3.0mm for subject 01, 02 and 03 (2^{nd} scan), 2.5mm for subject 03 (1^{st} scan), 04, and 05
[d] Acquisition matrix: 212x322

2.2.4 MRI sequences

Three different sequences acquired during the TIMBRE study imaging were relevant for the analyses performed for this thesis: a 3D T_1-weighted turbo field echo (TFE) with multi echo DIXON reconstruction (mDIXON), a coronal T_2-weighted turbo spin echo (TSE) with mDIXON and a coronal-sagittal interleaved acquired steady state free precession (SSFP) cine MRI. For readability, these sequences will be referred to as T1, T2 and cine respectively.

The T1 and T2 sequences were previously optimized for axillary lymph node imaging.[26] The cine MRI was never acquired interleaved before, therefore further optimization was necessary. Imaging parameters are shown in Table 2.2.

From the seven healthy volunteers one sagittal balanced SSFP (bSSFP) cine MRI was used for this study (Table 2.2).

The water-fat shift of the T1 was 0.3 pixel with an in-plane resolution of 1.25mm. Therefore, the actual shift was 0.38mm. For delineation purposes, a water-fat shift smaller than 1mm was considered adequate.

The T1 scans were used as reference image for lymph node delineation and interfraction motion quantification. The T2 was used for lymph node identification in combination with the T1. The cine scans were used for evaluation of intrafraction lymph node displacements. All scans were acquired in free breathing.

Optimization

For the T1 the field of view (FOV) size was enlarged after two patients because the heart and lungs (organs at risk) were not completely visible in de FOV. In the T2 the coronal slice thickness was changed from 3.0mm to 2.5mm. This was necessary for better brachial plexus visualization, since the T2 will eventually also be used for brachial plexus (which is an OAR) delineation. For the cine scan the acquisition order of the coronal and sagittal slices was changed after the first subject. A saturation band artifact resulting from the interleaved slice acquisition in the other direction remained present. This obscured the lymph node of interest, since the lymph node size was smaller than the saturation band, which is related to the acquired slice thickness. Therefore, the acquisition order of the cine MRI slices was changed, see section 2.3 Cine MRI saturation band artifacts.

Table 2.3: ***Number of completed scans per patient.***

Study ID	Number of scans			Patient repositioning
	T1	*T2 (slice thickness)*	*cine*	
01	3	1	3**	ELPS
02	2	1	2	*
03	2	2 (2.5mm, 3.0mm)	2	*
04	3	1	3	ELPS
05	2	1	2	*

Abbreviations: ELPS: external laser positioning system
* repositioning without ELPS
** cine MRI without 'yo-yo' stack order option

2.2.5 Acquired data

In Table 2.3 the number of acquired scans per study patient is shown combined with acquisition parameters that were not the same for all patients.

2.3 Cine MRI saturation band artifacts

In the cine MRIs of the healthy volunteers only sagittal slices were acquired. Compared to the interleaved acquisition of coronal and sagittal slices of the TIMBRE patients this is favourable in terms of temporal sampling resolution of the lymph node position: every 0.3 seconds a sagittal slice in the volunteer cine MRIs versus every 1.2 seconds (2* 0.6seconds) a sagittal slice in the TIMBRE cine MRIs. However, slice acquisition in a single orientation provides only 2D positional information, because the motion in the in-plane direction cannot be identified. Therefore, it was decided to use interleaved acquisition of orthogonal coronal and sagittal planes in de TIMBRE cine MRIs. This gives information about the lymph node position in 3D: superior-inferior and anterior-posterior in the sagittal planes, and superior-inferior and left-right in the coronal planes.

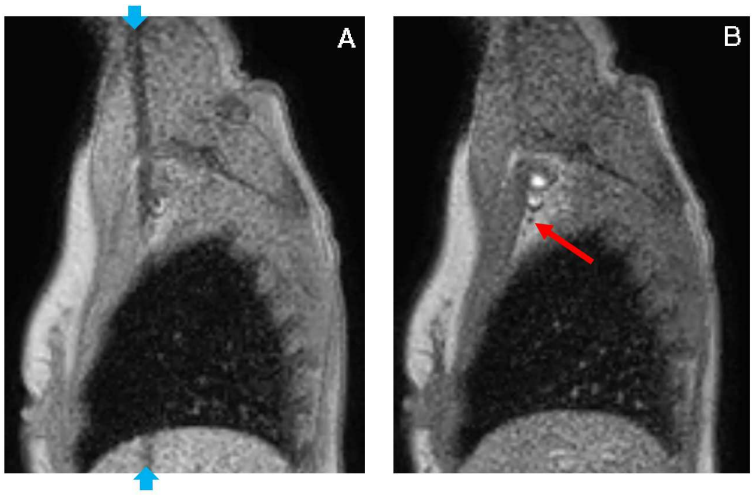

Figure 2.2: ***Cine MRI saturation band artifact.*** *A) The lymph node of interest is obscured by the saturation band artifact (between blue arrows) of the coronal slice that was acquired immediately before. B) In the second slice with the same orientation the saturation band has disappeared and the lymph node of interest (red arrow) is visible again*

In the first TIMBRE patient it was noted that a saturation band artifact through the lymph node of interest (Figure 2.2A) was visible in both slice orientations. The artifact obscured the lymph node. This artifact is caused by the excitation of the slice in the orthogonal direction that was acquired immediately before.

In order to acquire cine slices in which the lymph node is visible, the acquisition order of the cine MRI was adapted after the first patient. Instead of alternating a coronal (cor) and sagittal (sag) slice, the 'yo-yo' stack order option permitted cor–sag–sag–cor acquisition order. By this, two slices in the same direction were acquired directly after each other. In each second slice in the same orientation the saturation band artifact was not present any more (Figure 2.2B). This acquisition order permitted lymph node imaging in three directions simultaneously. However, a down side of this approach was a loss of temporal sampling resolution, because the slices with the saturation band artifact could not be used for lymph node position analysis.

3 Interfraction lymph node displacement

3.1 Introduction

In current regional RT (irradiation of axillary LNs) in breast cancer patients, the LN levels, called the clinical target volumes (CTV), are delineated according to consensus guidelines.[17] Delineation is done on CT and based on visualization of the breast, blood vessels, ribs and muscles, because individual LNs are not clearly visible. When using MRI individual LN identification becomes possible[26,27] (see chapter 1 General introduction). Therefore, the use of MRI, either as only imaging modality or added to CT, provides the possibility of delineating separate LNs as target volumes. Furthermore, it was shown that volumes of delineated individual LNs are much smaller than volumes of axillary CTVs.[27] That is why MRI could provide imaging that allows for redefinition of axillary CTVs to allow smaller target volumes.

With the introduction of radiation therapy techniques such as intensity modulated radiation therapy (IMRT) and volumetric modulated arc therapy (VMAT), highly conformal dose distributions around the target can be created. With the combination of a highly conformal dose and the aim for smaller targets and margins, magnitude of motion[32] and motion management become increasingly important. This is for instance relevant when aiming for smaller regional LN CTVs, for boosting of individual LN GTVs with small margins or for hypofractionated radiation schemes (with higher dose per fraction). Different error sources can be defined[33] that become more important in treatment preparation. These include displacement of the target volume with respect to the planning image, displacement of the skin with respect to the internal anatomy (when patient positioning is based on skin tattoos), set-up errors at each treatment fraction, and day-to-day variations in organ position.[33] All these error sources can lead to *inter*fraction displacement. This is displacement of a structure that is seen between images taken on two different treatment fractions.[32] Interfraction displacement can be random or systematic. Systematic interfraction displacement is the variation in position averaged over all treatment fractions compared with the reference image. Random errors are the variability in the displacement that is seen between images in all fractions.[32,34]

Systematic and random errors in displacements are incorporated in RT treatment plan preparation by using planning target volumes (PTV): a margin is added to the CTV to account for patient set-up and displacement uncertainties. Eventually, the aim for the MRI linac is to perfectly adapt the RT plan to the actual anatomy of the day and use MR imaging for real-time guidance and adaptation.[22,23,35] When online plan adaptation is realised, this will help in minimizing or completely eliminating those error sources. However, before this is realised adequate quantification and management of the errors mentioned is important.

In addition, when considering the use of MRI added to CT in the current workflow, only CBCT or electronic portal imaging devices (EPID) are available for set-up correction. Since individual LNs cannot be well visualized with these modalities it is important to consider the interfraction displacement of individual LNs for adequate choice of margins in treatment preparation.

Since individual LN visualization and identification has not been possible before use of MRI, displacements of individual LNs have never been studied before. Therefore, the goal of this chapter is to quantify the interfractional individual LN displacements. Sequential scans of the same patients

will be rigidly registered to each other to correct for differences in patient set-up. Next, differences in LN position between the scans are assessed. Two different local registration boxes will be used to investigate whether displacement of all individual LNs is similar or if separate LNs in different levels move independently of each other.

3.2 Methods and materials

3.2.1 Delineation

For the interfraction displacement analysis, all acquired T1 and T2 scans were used (acquisition described in chapter 2 Study population and MRI data), see Figure 3.1. Lymph nodes were identified on the T1 water-only and fat-only images and the co-registered T2 water image of the first set of scans of each patient. Manual delineation of the LNs was performed in the transverse slice direction on the T1 water image (Figure 3.1), using the in-house developed software programme Volumetool.[36] The fat image was used to check the delineation boundaries. All identified LNs and delineations were checked by a breast radiation oncologist (DvdB) and a breast radiologist (SdW). Subsequently, all identified LNs in the first T1 set were identified and delineated in the second and, if acquired, third T1 scan set of each patient as well.

In addition to delineation of the separate LNs, also the clinically used CTVs were delineated (Figure 3.1) and evaluated with a breast radiation oncologist. Delineation was done according to the clinically used delineation guideline for CT,[17] that was slightly adapted for use on MRI. These regional volumes are referred to as level 1 to 4. The interpectoral level was considered as level 2. A 1cm margin was added to each separate level to also incorporate LNs just outside a level. Lymph nodes that were inside the levels including the 1cm margin were considered relevant for analysis. All LNs were assigned to one level. If a LN was delineated on a boundary of two different levels, it was assigned to the level in which the largest part of its volume was delineated. If a LN was located only partially inside a level, it was considered to be included in the level.

3.2.2 Registration

To quantify regional displacement of the LNs within the body, and not the displacement of the whole body, local rigid image registration between all T1 MRI sets of each patient was performed using six degrees of freedom, allowing only translations and rotations. A registration based on normalized mutual information in a box-defined region of interest in the scan was used. This is performed with the VTK CISG Registration Toolkit (Kings College London, London, UK) via Volumetool.[36]

Two different registration boxes were used:

1. *Sternum box* (Figure 3.2A): a box in which the manubrium of the sternum is located, as well as the anterior part of the chest wall on the side affected by breast cancer, including ribs and muscles.

2. *Level 1 box* (Figure 3.2B): a more lateral box that is chosen more in the region of the level 1 LNs. It includes the lateral chest wall on the affected sides, including ribs, the pectoralis minor muscle, and part of the shoulder/arm muscles.

Registrations were checked visually on muscles, sternum, ribs and chest wall, and repeated when necessary.

The effect of the two different boxes on the registration of LNs in different levels was evaluated.

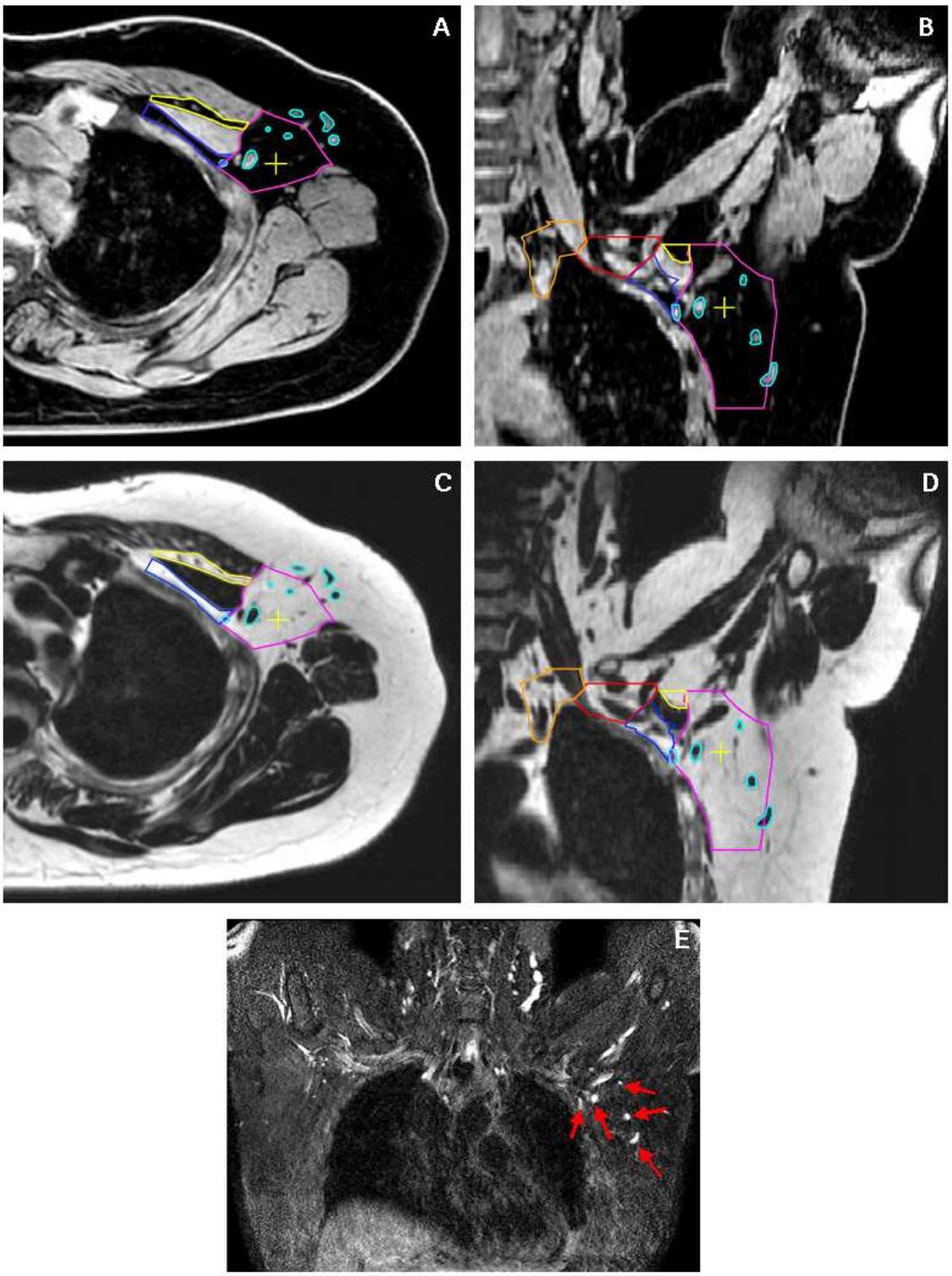

Figure 3.1: ***Images used for delineation of LNs.*** *A (transverse) and B (coronal) are a water-only image of the T1 TFE mDIXON MRI scan. C (transverse) and D (coronal) are a fat-only image of the same MRI scan. E is a coronal water-only image of the T2 TSE mDIXON. Separate LNs (light blue) and axillary LN levels (1-4) are shown (in pink: level 1, blue and yellow: level 2, red: level 3, orange: level 4). The red arrows indicate the same LNs in the T2 scan. The yellow crosshair indicates the intersection of the orthogonal planes.*

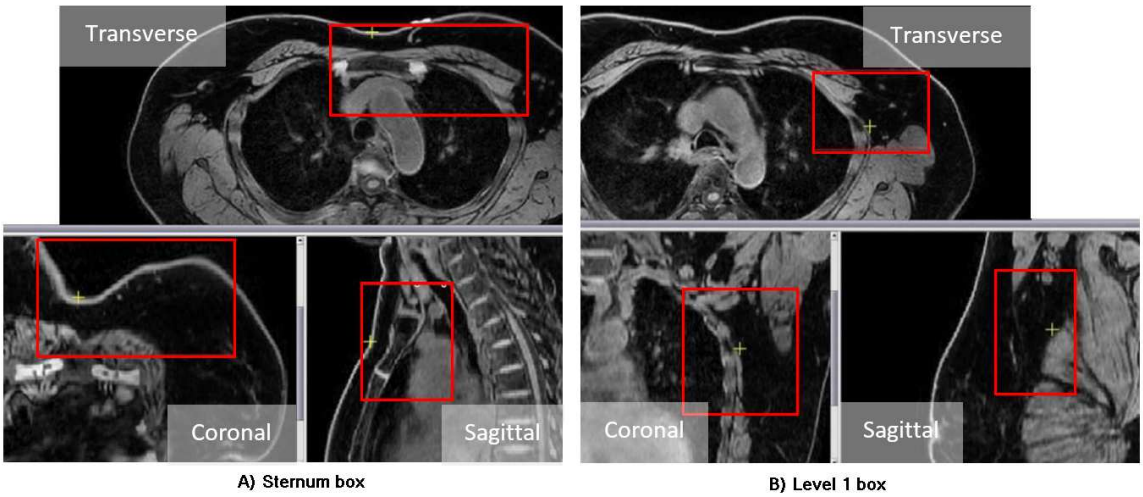

Figure 3.2: ***The two different boxes used for local registration.*** *The example shows a patient with left-sided breast cancer. In case of a tumour on the right side, the boxes were mirrored in the mid-sagittal plane.*

3.2.3 Quantification of displacement

After registration of the images, the inverse transformation matrices were used to transform the delineations of the LNs in the second and third scan of each patient back into the coordinate system of the first scan, which was used as reference. This was done using both the sternum box registrations and the level 1 box registrations. In the reference coordinate system, the centroids of the LNs were calculated. For an arbitrary LN with k delineated voxels, with 3D voxel coordinates $\mathbf{p}_1$, $\mathbf{p}_2$,...,$\mathbf{p}_k$, the centroid $\mathbf{c}$ is

$$\mathbf{c} = \frac{\mathbf{p}_1 + \mathbf{p}_2 + ... + \mathbf{p}_k}{k}. \tag{3.1}$$

The displacement $\mathbf{d}$ between the LNs in two scans of the same patients was calculated by

$$\mathbf{d}_n = \mathbf{c}_{n,set\ 1} - \mathbf{c}_{n,set\ i}, \tag{3.2}$$

where n is the number of the LN, i = 2,3. Set 1, 2 or 3 denotes in which scan the LN was delineated. $\mathbf{d}$ is a 3D displacement vector, which represents the displacement in left-right, anterior-posterior, and feet-head direction. The Euclidian distance is defined as the norm of this vector.

All processing was performed using MATLAB R2015a (The MathWorks, Inc., Natick, Massachusetts, USA).

3.2.4 Statistical analysis

A non-parametric Wilcoxon matched-paired signed rank test was used to assess whether delineated LN volumes in the different scan sets of a single patient were comparable. Furthermore, the same test was applied to assess the differences in the measured distances per LN level between the two registration boxes. A p-value smaller than 0.05 was considered statistically significant. GraphPad Prism 6.02 (GraphPad Software, Inc., La Jolla, California, USA) was used to perform all statistical tests.

3.3 Results

A total number of 12 T1 scans in five patients was delineated. 127 individual LNs were identified, the majority of which were found in level 1 (Table 3.1). 5 LNs were found outside clinically used LN levels, those were not taken into account in further analyses.

Table 3.1: *Number of identified LNs in all T1 scans.*

	ID	01	02	03	04	05	Total
	Total	**19**	**25**	**36**	**19**	**28**	**127**
Number of LNs	level 1	15	15	23	13	16	82
	level 2	1	2	1	2	1	7
	level 3	2	2	3	1	2	10
	level 4	0	4	9	2	8	23
	Other*	1	2	0	1	1	5
Number of T1 scans		**3**	**2**	**2**	**3**	**2**	**12**

* not taken into account in further analyses

An example of a T1 water image with delineated LNs and transformed LNs of the second scan (using the level 1 box) is shown in Figure 3.3. It is seen that the LN contours from the different sets generally show overlap although contours are shifted with respect to each other.

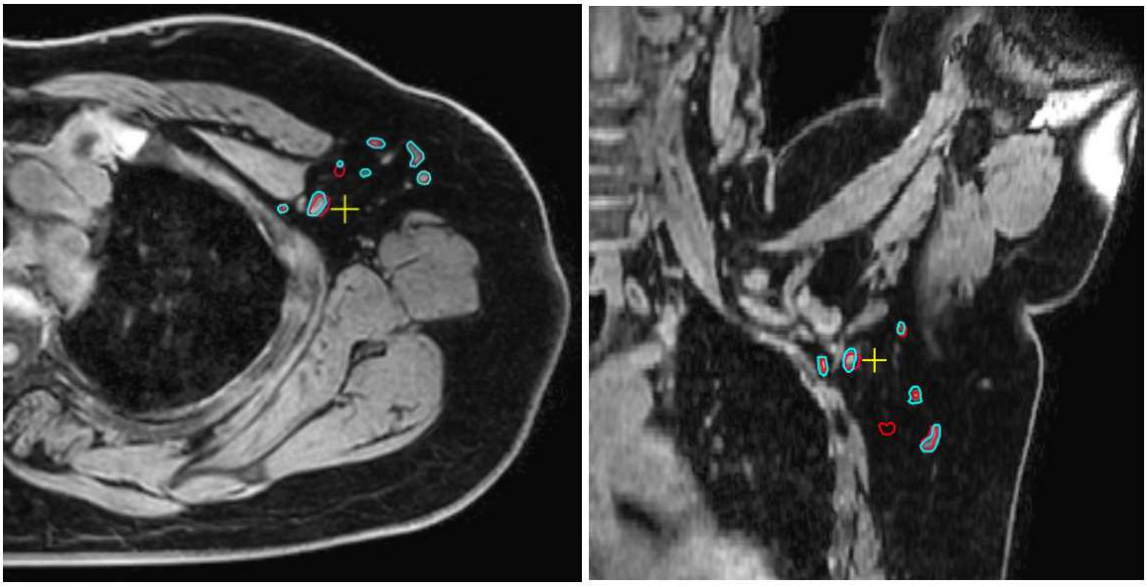

Figure 3.3: ***Example of delineated LNs (light blue) and transformed LNs (red) from set 2.*** *The blue contours are the delineations made on scan set 1, of which the images are shown. The red contours are the transformed contours transferred from scan set 2. The level 1 registration box was used for the registration. Left: transverse, right: coronal plane.*

Median LN volume was 0.093 mL (range: 0.020 mL minimum - 1.9 mL maximum) for the delineations of the LNs in set 1. For set 2 this was 0.088 mL (0.015–2.2 mL). The p-value of the Wilcoxon paired signed rank test was 0.082, the volumes were not significantly different. For the 38 LNs for which a third scan was available median LN volume was 0.092 mL (0.023-0.78 mL) in set 1 and 0.080 mL (0.021–0.60 mL) in set 3. This was also not significantly different, the p-value was 0.16.

Displacements between centres of gravity in all three dimensions are shown in Figure 4. The distribution is somewhat skewed around 0mm, especially for the sternum registration box in AP direction.

Euclidian distances and standard deviations of displacement per patient are shown in Table 3.2.

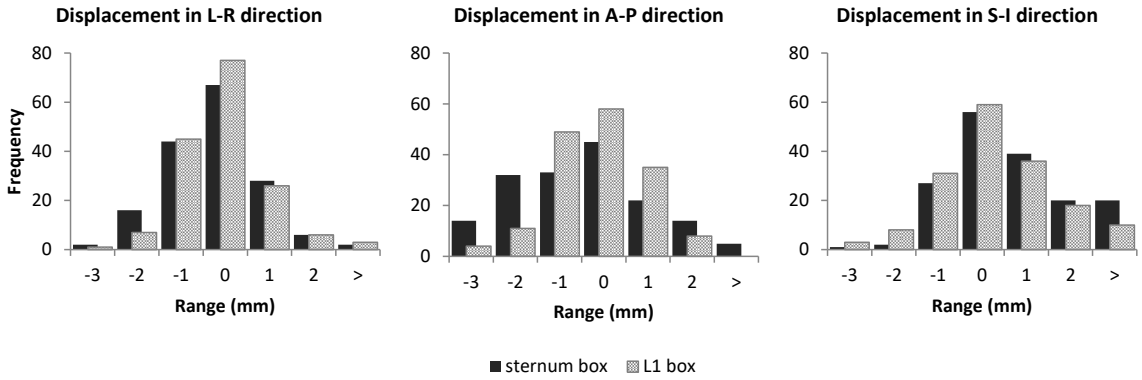

Figure 3.4: ***Histograms showing the distribution of centre of gravity displacement of the LNs in each direction.*** *The different colours represent the different registration boxes.*
Abbreviations: L: left, R: right, A: anterior, P: posterior, S: superior, I: inferior.

A mean LN displacement of 2.23mm was found for the sternum registration box, and 1.70mm for the level 1 box. Measured displacements differed per registration box. For the LNs in level 1 and 2, the level 1 registration box gave the smallest displacements (Table 3.2 and Figure 3.5). On the other hand, the sternum registration box resulted in smallest displacements for the LNs in level 3 and 4. These differences between the registration boxes were statistically significant for level 1 and level 4, p-values were < 0.0001 (Figure 3.5).

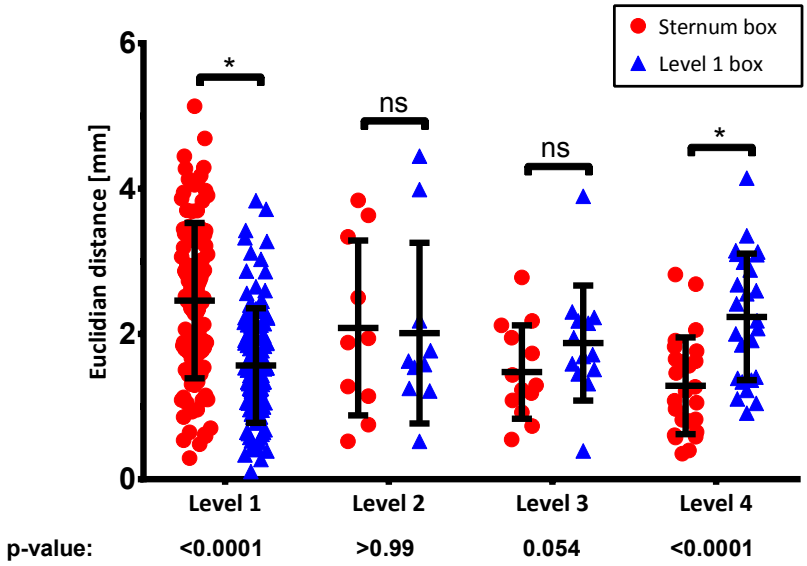

Figure 3.5: ***3D CoG displacement of each LN presented per level.*** *Each symbol represents the displacement of an individual LN. p-values of the comparison of the two different registration boxes are shown below the graph.*
* significant difference in paired t-test; ns: not significant

3.4 Discussion

In this chapter interfraction displacement of individual LNs was assessed on MR images in five breast cancer patients. Displacements of 1.55-2.47mm were found for LNs in different target levels. The choice of the local registration box proved to influence the measured distances. The sternum registration box resulted in smallest displacements for the level 3 and level 4 LNs, whereas the use of

Table 3.2: ***3D CoG displacement distances (SD) [mm] for the different registration boxes.*** *Results are shown per LN level. Green colour indicates which registration box resulted in the smallest displacement in each LN level.*

Registration box:		01 (set 1-2)	01 (set 1-3)	02	03	04 (set 1-2)	04 (set 1-3)	05	Mean
Sternum box	**Total**	**2.85 (1.05)**	**1.99 (0.62)**	**2.83 (1.34)**	**2.17 (0.84)**	**2.06 (0.70)**	**2.80 (0.77)**	**0.89 (0.39)**	**2.23**
	Level 1	3.16 (0.87)	2.03 (0.59)	3.55 (0.73)	2.54 (0.76)	2.20 (0.70)	2.93 (0.73)	0.90 (0.42)	2.47
	Level 2	1.86 (-)	1.28 (-)	3.48 (0.15)	0.75 (-)	2.22 (0.28)	2.86 (0.98)	1.14 (-)	1.94
	Level 3	1.08 (0.20)	2.03 (0.74)	0.96 (0.23)	1.17 (0.49)	1.09 (-)	2.12 (-)	1.18 (0.26)	1.38
	Level 4	-	-	0.75 (0.16)	1.72 (0.42)	1.49 (0.41)	2.29 (0.53)	0.76 (0.34)	1.40
Level 1 box	**Total**	**1.79 (0.76)**	**1.93 (0.70)**	**2.33 (0.73)**	**2.01 (1.10)**	**1.16 (0.59)**	**1.58 (0.38)**	**1.11 (0.45)**	**1.70**
	Level 1	1.84 (0.76)	1.83 (0.52)	2.08 (0.44)	1.68 (1.10)	1.02 (0.47)	1.46 (0.34)	0.93 (0.44)	1.55
	Level 2	0.52 (-)	1.21 (-)	4.22 (0.23)	1.25 (-)	1.65 (0.11)	1.88 (0.30)	1.63 (-)	1.76
	Level 3	2.06 (0.12)	3.10 (0.80)	1.93 (0.22)	1.68 (0.39)	0.39 (-)	1.45 (-)	1.64 (0.05)	1.75
	Level 4	-	-	2.48 (0.42)	3.05 (0.53)	1.98 (0.62)	2.09 (0.09)	1.29 (0.29)	2.18

the level 1 registration box lead to the smallest displacements in level 1 and level 2 LNs. Although these displacements are small, they are relevant to consider when aiming for conformal, high dose irradiation with small margins. In addition, it is necessary to define the registration box based on the localization of the targeted LNs.

Investigation of individual regional LN displacement in breast cancer patients with MRI has never been done before and therefore completely new information was acquired. The use of MRI is valuable because it enabled visualization of individual LNs and permitted three dimensional assessment of displacements. Because individual LN displacement was never assessed previously, no comparisons could be made with previous studies to evaluate the magnitude of the measured displacements.
However, optimal matching structures for whole breast and LN irradiation were previously investigated by Laaksomaa et al.[37,38] They investigated the influence of the matching positions of 2D orthogonal kV images on the patient set-up and found that a combination of the upper sternum, middle ribs and middle vertebrae resulted in best matching for the axillary LNs.[37,38] In this study we also investigated the influence of different registration positions. From the structures mentioned before, the upper sternum part lies within our sternum registration box and the ribs are included in the level 1 box. In our experience they also provided good structures for matching of the scans.

A strength of our method is the use of the centre of gravity as reference of the LN position. Different studies investigating motion of lung tumours and mediastinal LNs or mediastinal LN levels used an approach that was comparable to the one we used,[39–41] therefore the approach we used seems feasible. Our approach was similar because in these studies also the centres of gravity of structures of interest were compared to a reference image and because 3D information was obtained. On the other hand, these studies were CT-based and used registration on bony anatomy, except for Weiss et al.[40] who additionally used soft tissue registration. We used MRI and therefore a region of interest registration algorithm based on all structures and mutual information. This could lead to different registration accuracy. The advantage of MRI compared to CT is the improved soft tissue contrast which is necessary to visualize the individual LN.
An advantage of the use of the centre of gravity is that local variations in delineation of LN boundaries are averaged. Delineation uncertainty mainly existed in the transverse plane that was used for delineation. A difficulty sometimes was to decide in which transverse slice to end the delineation. As mentioned, the centre of gravity will average part of this uncertainty. Nevertheless, reconstructed slice thickness was 1.25mm, and LNs are small structures. So the decision in which slice to stop can still be of influence on the centre of gravity position in superior-inferior direction. In addition to that, only one observer delineated the LNs. Therefore, intraobserver variation in delineation of the

different scan sets can be present. Also for this it is expected that the use of the centre of gravity reduces the influence of the intraobserver variation between different scan sets of the same patient. Furthermore, because in total 127 LNs were used to determine the interfraction displacements, the delineation uncertainties and intraobserver variations will also be averaged over all the LNs which will further decrease their impact on the measurements.

A disadvantage of transforming the LN delineations the other scan sets back to the reference image is that the contours had to be transformed to a different voxel grid. With this transformation delineation accuracy was lost. However, it was checked that centre of gravity position was not influenced by the grid. Therefore, the transfer of the contours did not influence the calculation of LN displacement.

It is important to carefully check the registration between the scans because errors in the registration will directly lead to different measured displacements. Visually the registrations seemed good and in case of doubt the registration was repeated. However, it was done by only one observer. For an extension of the LN displacement analysis to more patients it could be valuable to ask a separate observer to check the registrations.

A point of uncertainty that remains is the identification of LNs since there is no gold standard that could confirm the identification. LN Identification was performed by one observer (MGK), but two other observers, a breast radiologist (SdW) and a breast radiation oncologist (DvdB), checked all identified LNs and searched for missed LNs. Nevertheless, structures could still be misidentified or LNs missed. Especially, for structures close to muscles and blood vessels it was not always clear whether or not it were LNs. However, all observers agreed for the majority of structures and all structures were detected in all scans of the same patients. In the end, all structures that were considered as LNs were therefore based on consensus of three observers. Therefore, planned analyses for this work could all be performed and the results give a good representation of the LN displacements.

The registration of MRI images simulates image-guided patient set-up and correction of set-up errors as would be done in treatment procedures. Although it is different than set-up correction in current clinical practice, the use of two different registration boxes is another strength of this study. It permitted assessment of the influence of the matching position on LN displacement relative to the reference image.
In initial analyses it was seen that the sternum box registration performed very well for level 3 and 4 regions, but a structural displacement of the LNs in one direction remained present in level 1 (see Figure 3.4 and Appendix Figure A.1). The level 1 box which is situated more towards the level 1 position shows less movement for level 1 and 2, but more in level 3 and 4 compared to the sternum box. This shows that LNs in different levels move independently from each other. A possible explanation for this is that LNs are small structures situated in a soft fatty tissue region that is very deformable. Change in arm and shoulder muscle position relative to the ribs and sternum results in different change in position of the level 1 and 2 LNs compared to the level 3 and 4 LNs.
Influence of arm position on LN position has been previously assessed. It was a study of Dijkema et al.[42] that performed a qualitative evaluation of the influence of adduction or abduction. They found that LN position changed with arm position. Our patients were all scanned with arms in abduction and there were no large differences in arm position between the scans. However, possibly small differences in arm position of patient set-up also influence LN position. This can be an explanation for the differences in registration per LN level that were found in this study with the different registration boxes.

The observation that the displacements of LNs depended on the choice of the registration box is important. It indicates that for individual LN irradiation position verification has to be performed locally. Magnitudes of measured LN displacements can therefore not directly be translated into current clinical practice because local RT to the breast is always part of the same treatment plan as the regional RT. Therefore, in clinical practice the position verification is for breast and LN levels si-

multaneously and a different registration position for set-up correction is used than the registrations boxes we chose here.

To conclude, interfraction displacement of individual LNs was quantified and was found to be small. This first investigation of interfraction displacement is relevant when aiming for individual LN irradiation with a high dose, small margins and hypofractionated treatment. Eventually, such an approach may lead to a possible reduction in side-effects and toxicity. It has to be further investigated how to take into account these displacements.
When considering MRI in combination with the current CT-based workflow, MRI might help in facilitating delineation of the target LNs. Interfraction LN displacements then have to be taken into account in planning margins, the PTV. A larger population and analyses of more scans is necessary to gather enough data for determination of these margins. A PET scan will be necessary for identification of tumour-positive LNs. It has to be evaluated what the contribution of MRI in combination with CT and PET-CT is to the delineation of LN (boost) target volume. This will be further investigated in the TIMBRE patient study.[31]
When aiming for an MRI-only workflow and (positive) LN irradiation on the MRI linac, an approach has to be developed to adapt the delineations and the treatment plan based on the anatomy of the moment. Initially, this could also be covered by adding margins. Eventually, it is desirable to adapt the delineations and the treatment plan to the actual anatomical situation, such that interfraction displacements play no role any more. This is one of the reasons for a first exploration of intrapatient contour propagation that is described in chapter 5.
For both approaches (MRI added to CT workflow and LN RT on the MRI linac) it is important to consider how to perform position verification of the patient since it was shown that the choice of registration position influences the magnitude of the measured displacement.

Another factor that influences the accuracy of dose delivery and should be considered for high boosts with small margins is intrafraction LN motion. This topic is addressed in the next chapter.

3.5 Conclusion

Interfraction displacement of individual axillary LNs in breast cancer patients was quantified. Movements up to 2.5mm average displacement for level 1 LNs were measured using local registration boxes. Differences in displacement magnitude were found for LNs in different levels. These were depending on the position of the box used for image registration. Therefore, it is important to very locally verify target position when aiming for hypofractionated individual LN boosting. Although the observed displacements were small, they have to be taken into account when working towards a highly conformal RT approach of individual LNs.

4 | Intrafraction lymph node displacement

4.1 Introduction

In addition to *inter*fraction displacement, *intra*fraction motion is another important factor to consider when aiming for irradiation of individual lymph nodes. Intrafraction motion is the motion of the target volume seen within the time frame of a single treatment fraction.[32,43] Different components contribute to intrafraction motion. These include internal organ motion, patient movement, and respiratory motion,[32,43–45] as well as movements caused by the skeletal muscular or cardiac system.[45]

Movements of target volumes during irradiation may lead to decreased target coverage and an increased dose to surrounding organs. When reducing the number of fractions, higher doses per fraction are given. These can result in an increase of treatment time per fraction compared to conventional fractionated treatment. In addition with aiming for smaller margins with improvements in image guidance, this makes that intrafraction motion management becomes increasingly important.

With cine MRI it is possible to acquire images with good soft tissue contrast and sufficient temporal resolution, making it perfectly suitable to study intrafraction motion.[29,46–48] The MRI linac provides the possibility of real-time intrafraction imaging without additional imaging radiation dose,[22,35,47] thereby facilitating tumour motion tracking during irradiation. This gives the opportunity to increase the conformity of the dose without missing the target.

Before online motion management strategies are accessible, or to develop these, it is important to understand the magnitude and characteristics of the motion of your target during treatment. In this chapter the intrafraction displacement of individual axillary lymph nodes is evaluated using cine MRI to gather this information.

Several other studies investigated organ motion on different time scales. These studies examined for instance prostate and organ at risk motion,[49] pancreatic tumour motion,[50] or GTV and CTV motion in rectal cancer patients.[46] Deformable image registration was used to quantify the motion. One of the chosen approaches was an optical flow algorithm.[50] These studies showed that deformable image registration is a feasible method to study organ specific motion. Furthermore, they demonstrated that variations in motion between organs and patients can be found.[49,50] Therefore, we also chose to use an deformable image registration method for the investigation of intrafraction LN displacement.

4.2 Methods and materials

All patients underwent cine MRI scanning as described in chapter 2 Study population and MRI data. Cine MRIs in which no lymph nodes were visible were not considered for analyses. All processing was performed using MATLAB R2016a (The Mathworks, Natick, MA).

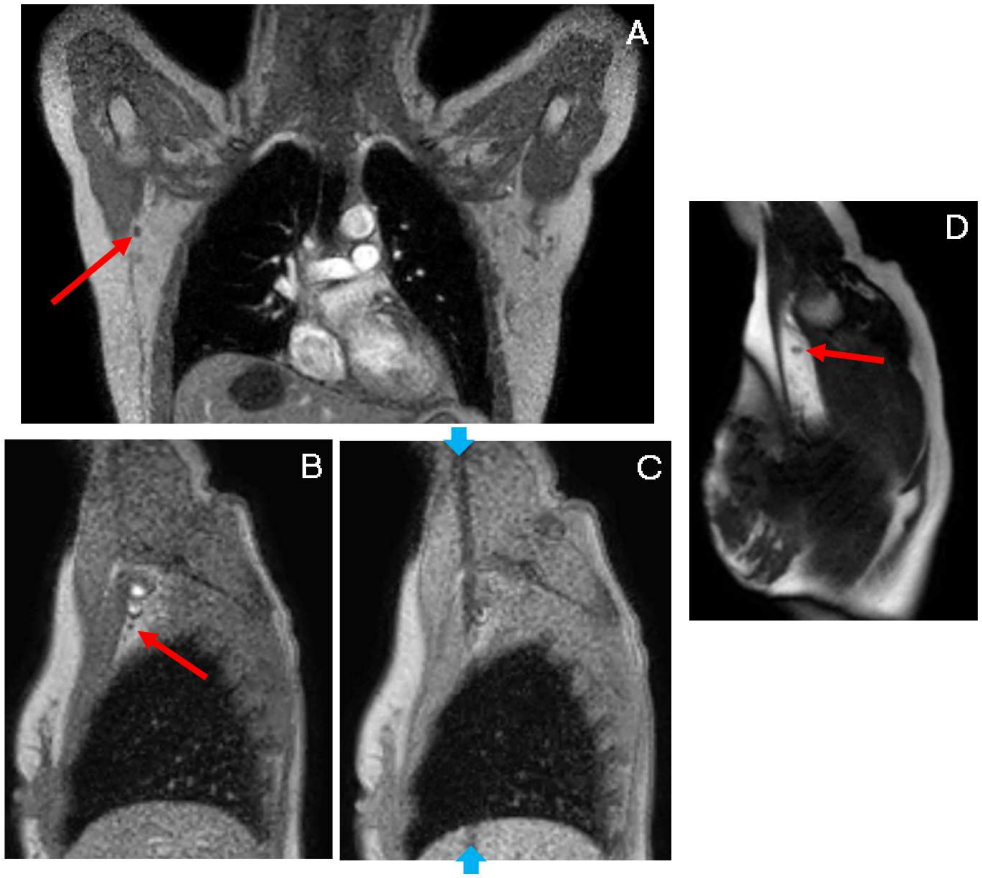

Figure 4.1: ***Example of coronal and sagittal frames of cine MRIs.*** *A) shows a coronal image and B-D) sagittal images. C) shows a sagittal frame with a saturation band (between blue arrows) from the coronal frame that was acquired interleaved immediately before. In this frame the LN is obscured by the saturation band. A-C) are cine MRIs from the TIMBRE study, D) is a cine MRI from a healthy volunteer. The red arrows indicate the lymph node of interest.*

4.2.1 Image registration and motion quantification

Pre-processing TIMBRE cine MRIs

The motion of the lymph nodes was investigated by registering all cine MRI frames (Figure 4.1) to a reference frame (the 10^{th} of all slices). Before image registration was carried out, a couple of image pre-processing steps were performed (Figure 4.2). Every other slice of all cine images was removed because a saturation band artifact (section 2.3 Cine MRI saturation band artifacts and Figure 4.1C) through the lymph node of interest caused by the interleaved orthogonal acquisition made those images unusable. Furthermore, the saturation band artifact complicated the registration with the algorithm that was used. This slice removal resulted in a reduction in temporal resolution of the analysed time points, to half of the acquired temporal resolution (from an image every 0.6s to every 1.2s). Subsequently, the image was cropped to a smaller rectangular image to decrease image size for faster processing. The image was resampled with cubic interpolation to double resolution for smaller pixels and a smoother image, and to increase the number of pixels per lymph node. The contrast in the image was enhanced by saturating the high intensities based on the maximum intensity of the cropped reference image. Additionally, the image was smoothed with a Gaussian filter with a kernel with standard deviation 1 to reduce the noise level.

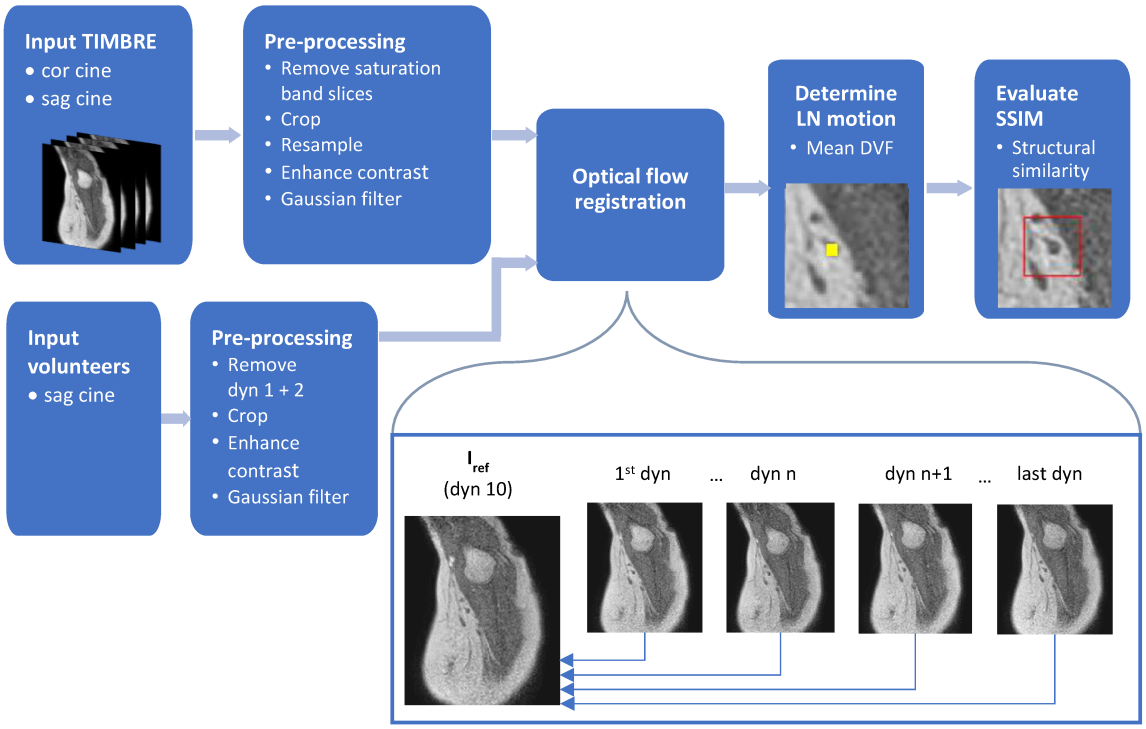

Figure 4.2: ***Flowchart showing the different steps of the intrafraction analysis process.*** *As input coronal or sagittal cine MRI series are used. Different pre-processing steps are performed to make the images suitable for the optical flow registration algorithm. The images are registered to a reference image (I_{ref}, the 10^{th} dynamic) using the optical flow algorithm[51,52] which results in DVFs. The LN displacement is quantified by taking the mean DVF of the pixels in the lymph node area. Finally, registration quality (inside the red box around the LN) is assessed by SSIM.[53]*

Abbreviations: cor: coronal, sag: sagittal, dyn: dynamic, DVF: deformation vector field, SSIM: structural similarity measure.

Pre-processing volunteer cine MRIs

From the cine MRIs of the healthy volunteers, no slices had to be removed because of saturation bands, because images were only acquired in the sagittal plane (see chapter 2 Study population and MRI data). In each cine the first two acquired slices were removed to avoid influence of the brighter pixel intensities in these slices on the lymph node tracking. In contrast to the TIMBRE cines no pixel resampling was performed, as pixels in these cines were already small enough. See also Figure 4.2.

Displacement quantification

After pre-processing, all frames in the cine MRI series were pixel-wise deformably registered to a reference frame of the same series (the 10th dynamic of the series). This was done using an optical flow algorithm.[51,52] An alpha factor (weighting of sensitivity between grey level intensity variation and regularity along space) of 0.35 was chosen empirically by testing a small subset of all cine images. The optical flow algorithm resulted in a deformation vector field (DVF), which gives a displacement vector from the test frame to the reference frame for each pixel.

To quantify the lymph node displacement, a rectangular region of pixels belonging to the lymph node of interest was selected manually (Figure 4.2). The mean of the deformation vectors of these pixels was taken as representation of lymph node movement with respect to the reference image. The coronal images were used to quantify displacements in left-right (LR) and superior-inferior (SI) direction, whereas anterior-posterior (AP) and SI displacements were evaluated on the sagittal images. The maximum distance measured between all lymph node positions (or the range of motion)

is reported as the intrafraction displacement in all directions. This ensures that respiratory motion as well as motion drifts are incorporated in the measurement.

4.2.2 Registration accuracy

To evaluate the quality of the performed registration a structural similarity (SSIM) measure[53] was used. This was only evaluated locally around the lymph node of interest (Figure 4.2). Only the structural component of this similarity measure is used, after normalization for luminance and contrast. For all frames the structural similarity is determined with respect to the reference frame. This is calculated by

$$S = \frac{1}{N}\sum_{i=1}^{N}\left(\frac{\sigma_{12,i}+C}{\sigma_{1,i}\sigma_{2,i}+C} \right), \tag{4.1}$$

in which S is the structural similarity level, between 0 (no similarity) and 1 (perfect similarity), σ_1 the standard deviation in the reference image and σ_2 the standard deviation in the compared frame. $\sigma_{1,2}$ is the correlation between the reference and compared frame after luminance subtraction and variance normalization. C is a constant used for stabilization of the fraction,[53] it was set to 0.021. The σ's are calculated for small windows of 3x3 pixels in the region of the lymph nodes. Therefore, to determine a single S per frame, the values were averaged over all N 3x3 pixel windows.

4.2.3 Statistical analysis

A paired t-test was performed to test whether the difference in SSIM in all cine frames before and after optical flow registration was statistically significant. A p-value smaller than 0.05 was considered significantly different. Statistical test were performed with GraphPad Prism 6.02 (GraphPad Software, Inc., La Jolla, California, USA).

4.3 Results

From the total number of 12 acquired cine MRI scans in five study patients, 7 scans were included for intrafraction lymph node analysis. Scans of patient 01 were not included in analyses, because all coronal and sagittal slices showed a saturation band due to the acquisition order. In the other scans that were not included the lymph node was not visible in the acquired cine slice. From all seven healthy volunteers, one cine MRI per volunteer was analysed.

In Figure 4.3A a lymph node displacement trajectory of a sagittal cine scan of a TIMBRE patient is shown. In this patient a maximum displacement of 2.4mm in AP direction and 2.3 mm in SI direction was found. In Figure 4.3B another LN trajectory is shown of a healthy volunteer scan. A maximum AP displacement of 2.6 mm and a 1.2 mm SI displacement were found. A slight drift in breathing level is visible in AP direction. In Figure 4.4 the displacements from the same TIMBRE patient, but now combined in AP and SI direction, are plotted on top of the reference image. This gives an idea of the scale of the measured lymph node motion relative to the acquired voxel size.

Maximum lymph node displacements measured in all patients were between 1.2 and 2.0 mm in LR, 0.9 and 2.5 mm in SI 1.1 and 2.6 mm in AP direction. For the healthy volunteers this was between 0.9 and 2.2 mm in SI direction, and 1.2 and 3.2 in AP direction (Table 4.1).

Structural similarity (SSIM) per dynamic before and after optical flow registration of the same patient and volunteer as in Figure 4.3 is shown in Figure 4.5. Mean SSIM values for all cine MRIs are shown in Table 4.2. A mean improvement after registration from 0.88 to 0.93 in coronal cine images, and from 0.79 to 0.88 in sagittal images was seen in the TIMBRE study cine MRIs. For the healthy volunteer cine MRIs mean SSIM changed from 0.94 to 0.98. All SSIM values increased statistically significant.

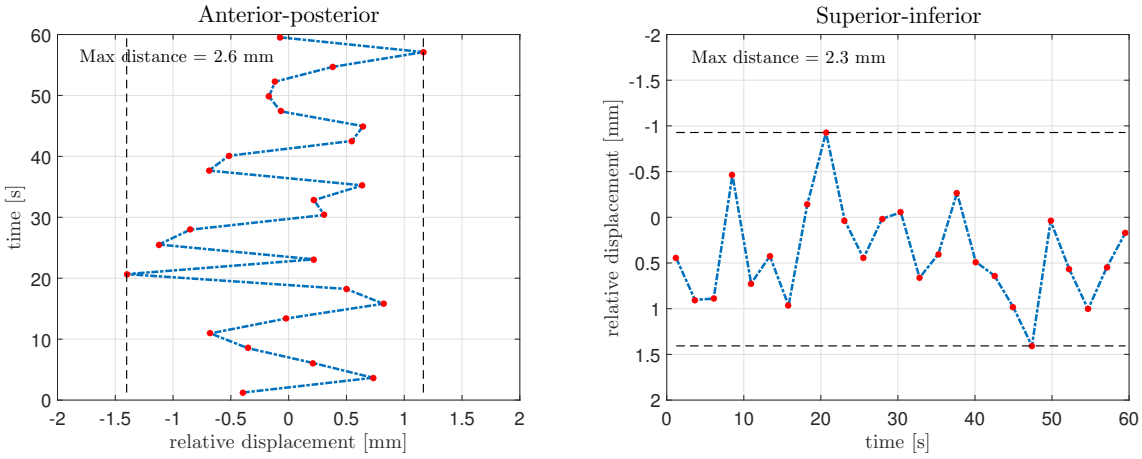

(A) *TIMBRE patient*

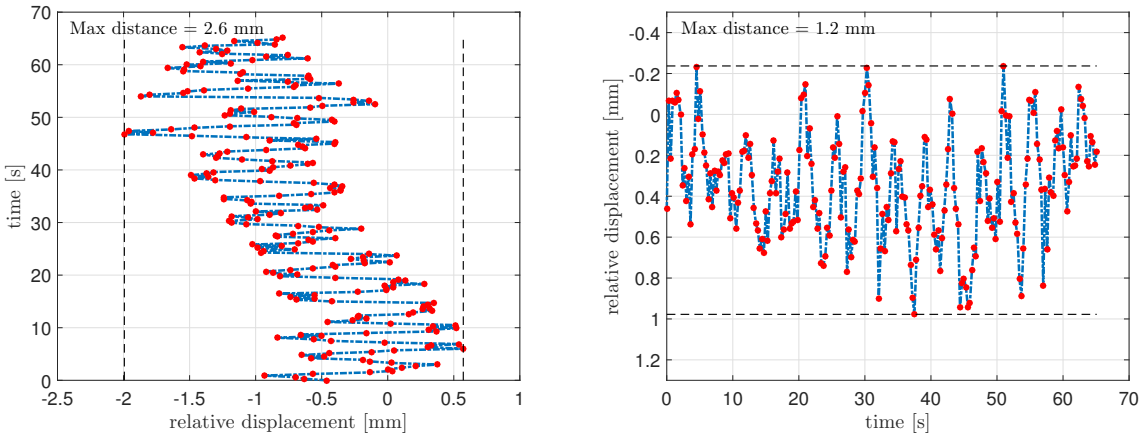

(B) *Volunteer*

Figure 4.3: ***Example of measured lymph node displacements in sagittal cine MRIs of a study patient (A) and a volunteer (B).*** *The picture on the left shows the displacement in AP direction [mm] and the right image in SI direction. The red dots indicate the measured time points. The extrema of the measured positions are indicated with the dotted black lines. The distance between these lines is taken as maximum displacement in the respective direction. Note that the axes limits differ between A and B and that the time and displacement axes are swapped between AP and SI. This was done to show the LN displacement in the same direction as visible on the cine image.*

Table 4.1: ***Intrafraction LN displacement (SD) [mm] in seven study (left) and seven volunteer (right) cine MRIs.***

ID (TIMBRE)	Series #	Coronal		Sagittal		LN level
		LR	SI	SI	AP	
02	301	2.0	1.4	1.6	1.9	1
	1901	1.3	1.6	1.9	1.2	1
03	401	1.3	1.3	2.1	1.7	1
	1001	1.9	2.4	2.5	2.4	3
04	1801*	1.6	1.5	2.3	2.6	1
05	501	1.2	1.0	0.9	1.1	1
	901	1.7	1.5	1.2	1.6	1
Mean		**1.6 (0.29)**	**1.5 (0.40)**	**1.8 (0.54)**	**1.8 (0.52)**	
			1.7 (0.49)**			

ID (volunteers)	Sagittal		LN level
	SI	AP	
V1	0.9	1.2	1
V2	1.8	1.3	1
V3	1.2	2.6	1
V4	2.2	1.9	1
V5	1.8	3.2	1
V6	2.1	2.4	1
V7	1.7	2.4	1
Mean	**1.7 (0.43)**	**2.1 (0.67)**	

Abbreviations: LR: left-right direction, SI: superior-inferior direction, AP: anterior-posterior direction.
* Not the same LN in cor and sag slices.
** Combined mean of coronal and sagittal measured maximal SI motion amplitude.

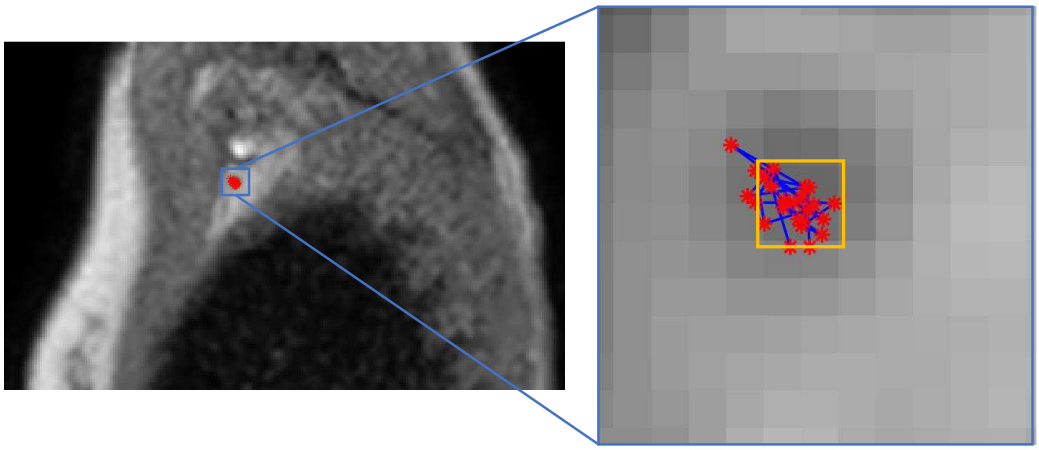

Figure 4.4: ***Lymph node trajectory plotted on top of reference cine image.*** *On the left the lymph node trajectory in a TIMBRE cine MRI found with optical flow is plotted on top of the cine image that was used as reference. On the right a zoom in of the area indicated on the left image is shown. The pixels shown here are already an interpolation of the originally reconstructed pixel size. The orange box indicates the acquired voxel size.*

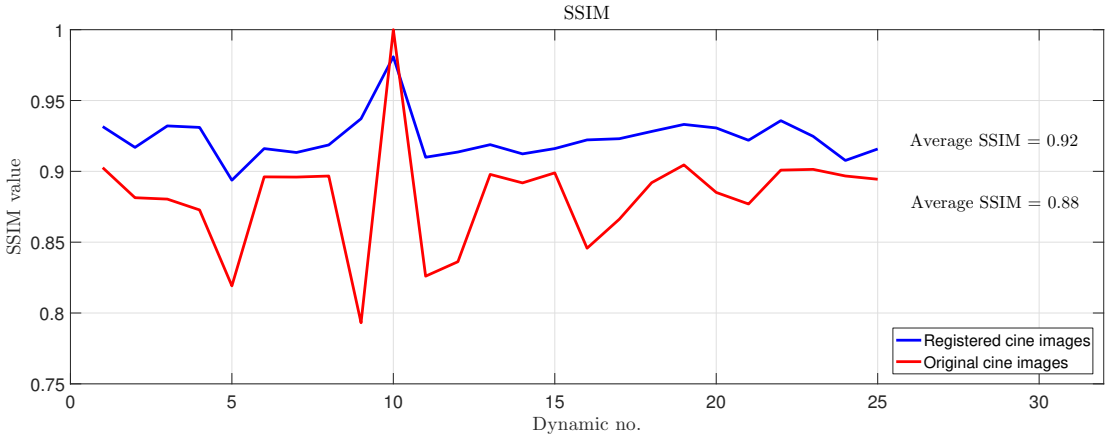

(A) *TIMBRE patient*

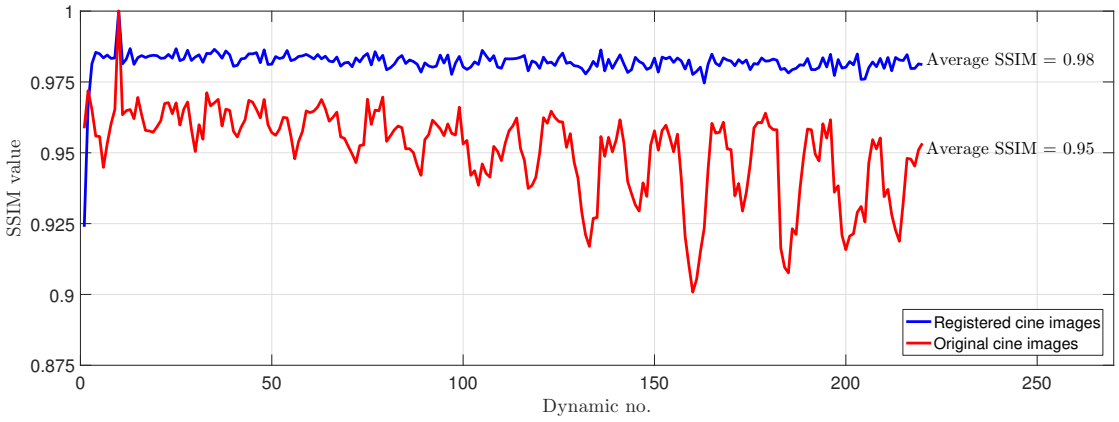

(B) *Volunteer*

Figure 4.5: ***Structural similarity before and after optical flow registration in a study patient (A) and a volunteer (B).*** *The red line shows the SSIM for the unregistered images, the blue line for the images after registration with optical flow. Dynamic number 10 was used as reference image. An increase in SSIM is seen after registration.*

Table 4.2: ***Mean SSIM for all cine MRIs before and after optical flow registration.*** *A statistically significant increase of SSIM is observed due to registration. Left: TIMBRE, and right: volunteer SSIM values.*

ID (TIMBRE)	Series #	Coronal			Sagittal			ID (volunteers)	Sagittal		
		Unregistered	Registered	p-value	Unregistered	Registered	p-value		Unregistered	Registered	p-value
02	301	0.94	0.96		0.88	0.93		V1	0.95	0.98	
	1901	0.96	0.98		0.88	0.93		V2	0.94	0.98	
03	401	0.91	0.93		0.78	0.87		V3	0.95	0.98	
	1001	0.92	0.95	<0.0001	0.88	0.94	<0.0001	V4	0.95	0.99	<0.0001
04	1801	0.91	0.95		0.88	0.92		V5	0.92	0.97	
05	501	0.94	0.95		0.91	0.96		V6	0.92	0.97	
	901	0.93	0.95		0.86	0.89		V7	0.97	0.99	
Mean		**0.93**	**0.95**		**0.87**	**0.92**		**Mean**	**0.94**	**0.98**	

4.4 Discussion

In this chapter intrafraction displacement of individual axillary lymph nodes was investigated. In seven cine MRIs of five TIMBRE study patients the mean range of motion (standard deviation) was 1.6 (0.29) mm, 1.7 (0.49) mm, and 1.8 (0.52) mm in LR, SI, and AP direction respectively. In seven healthy volunteers this range was 1.7 (0.43) mm in SI direction, and 2.1 (0.67) mm in AP direction. The shape of the LN trajectories indicated that LN motion mainly originated from breathing motion. In the displacement trajectories small drifts but no large patient shifts were observed. This indicates that although the displacement amplitude is small, still LN motion is present within the time frame of a single fraction. This is relevant to consider when targeting individual LNs and aiming for margin reduction.

At the moment of writing this is the first investigation of intrafraction displacement of individual LNs. Two studies[44,54] were found that have examined motion of lymph node levels on four dimensional CT (4DCT) data. Qi et al.[44] reported maximum centroid movements during normal breathing ranging from 1.4 to 3.4mm. Average maximum centroid movements (SD) with respect to the reference breathing phase (20% in 4DCT) of 1.9 (0.8) mm in LR direction, 0.2 (0.4) mm in SI direction, and 1.3 (0.5) mm in AP direction were found. Moran et al.[54] measured short-term displacement of the infraclavicular (ICV) and supraclavicular (SCV) nodal regions. These are equal to our levels 3 and 4. For the ICV nodes they found LR displacement of 0.0 (0.5)–0.2 (1.0) mm, AP displacement of 0.4 (1.6)– -2.2 (2.5) mm, and SI displacement of 0.5 (1.5)– -1.9 (2.2) mm for normal breathing (defined as 20–40% of vital capacity). For the SCV nodes these were in 0.4 (0.7)–0.5 (1.3) mm, 0.4 (1.1)–1.3 (1.9) mm, and 0.6 (1.0)– -0.3 (1.0) mm in LR, AP and SI direction respectively. For both studies no information on the delineation guidelines of the axillary levels was provided. The results of both studies during normal breathing are in the same order of magnitude as our results. However, since motion of lymph node levels was reported it is not clear whether these findings can be directly translated towards individual LNs.
Additionally, Moran et al.[54] reported maximum displacements for deep breathing (at 80% of vital capacity) up to -11 mm of ICV nodes and up to -10 mm of SCV nodes in AP direction. This is much larger than what we found, which can be explained by the fact that we did not assess deep breathing. Nevertheless, the magnitude of these displacements underline the relevance of motion assessment and management when moving towards highly conformal RT of individual LNs.

The studies mentioned hereabove[44,54] showed that LN motion is largely induced by breathing motion. This is also visible in the periodic shape of our LN movement graphs (Figure 4.3). However, in some patients also a slight baseline drift was visible (Figure 4.3B in AP direction). This resulted in a larger maximum amplitude than the actual amplitude of a breathing cycle. On the time scale of a single treatment fraction, such drifts may eventually result in a larger overall target displacement than the breathing motion amplitude itself because the target may drift away from the set-up position. This can result in an undesired decreased target coverage and an increase of dose to the organs at risk. For breast cancer RT a 1.3mm posterior drift of the sternum within a single treatment

fraction was seen in a recent study.[55] This drift was attributed to muscle relaxation. This type of baseline drift could possibly play a role in LN irradiation and dose distribution as well. Therefore, not only the amplitude of breathing motion is relevant to consider. In this study baseline drifts were also considered, because the maximum peak-to-peak amplitude was reported. This includes breathing motion amplitude as well as baseline drifts.

The use of cine MRI allowed for studying the LN motion on a scale of seconds. This enabled the detection of baseline drifts and periodic displacement caused by breathing motion. However, by the removal of the cine slices with the saturation band artifact, the temporal resolution of the available images was halved in the TIMBRE patients. When comparing Figure 4.3A and 4.3B, it is evident that with the higher sampling rate of the volunteer images, the respiratory motion path is more clearly visible. Taking in mind the sampling theorem,[56] which states that a sufficient sample rate is at least two times higher than the highest frequency of the measured signal, the remaining temporal resolution of the cine MRI might have been too low to completely cover the respiratory motion. We acquired 25 slices per minute in each plane. This means that if the breathing rate of the patients was higher than 12 per minute, detected LN displacements may not represent real motion, because of aliasing. Unfortunately, LN position tracking was not possible in the slices with the saturation band artifact because it obscured the LN. Therefore, removing these slices was considered feasible. Furthermore, it would not have been feasible to improve temporal resolution by decreasing the spatial resolution since voxel size was already large compared to LN size and measured displacements. Alternatively, coronal and sagittal images could be acquired sequential instead of interleaved since no saturation band artifacts will then occur. However, we chose not to do this, because sequential acquisition does not facilitate simultaneous assessment of motion in all three directions.

Our optical flow tracking results were only verified by visual inspection of the cine MRIs. No validation was performed by comparing it to manual tracking results or phantom measurements. However, the accuracy of optical flow has been previously studied, and an accuracy of 0.4mm-0.8mm[51,57] was reported. Additionally, in a study where it was compared to manual tracking, the error was the same size as image resolution[52] which is the precision limit for manual tracking. Because optical flow uses a smooth motion constraint and assumes similar displacement vectors for adjacent pixels[57] subpixel accuracy can be obtained.[57] Although LNs are very small structures, we could use a couple of pixels per LN to calculate the displacement. We assume that the average motion of the LN pixels represented the LN displacement fairly well. Since the displacements we measured were often smaller than the acquired voxel size, LN motion tracking by hand probably would not have been more accurate. Therefore, the choice of the optical flow algorithm was feasible. However, the measured subvoxel displacements illustrate that the limiting factors of the MRI acquisition in terms of in the voxel size might influence measurement accuracy more than the accuracy of the optical flow algorithm.

In the current data only one LN outside level 1 was imaged. During MRI acquisition it proved difficult to quickly identify LNs outside level 1 and plan the cine slice acquisition in a different LN level. It is therefore not clear whether displacement magnitude and motion pattern of LNs in different levels are the same as we found here. The patients and volunteers in this study had no positive LNs. Tumour-positive LNs can be larger than LNs without metastases. Therefore, the inclusion of patients with tumour-positive LNs outside level 1 in the study can possibly help in identifying and studying the motion of LNs in different levels.

Furthermore, it could be interesting to extend the length of the cine MRI acquisition. The current cine MRIs were acquired during approximately one minute only, but actual treatment times will be longer than one minute. A longer acquisition would give a better idea of actual intrafraction motion on the time scale of a single treatment fraction. Possible other factors than breathing motion only, such as baseline drifts or patient relaxation, will play a bigger role on a longer time scale and will then become apparent.

In conclusion, this research gave a first impression of 3D displacement of individual axillary LNs. This is useful information to guide workflow development for highly conformal hypofractionated RT aimed at an individual LN approach on the MRI linac. At present, only offline analyses of the cine MRIs were performed. For the application of motion management during irradiation real-time tracking[47,51,57,58] or accurate motion prediction[48] has to be realized. These methods should be robust to baseline drifts and sudden patient movement, caused for instance by coughing. Eventually, the ultimate method to compensate for intrafraction motion would to adjust the radiation beam[59] or to gate the delivery[60] based on real-time tracking of the target. Ideally this eliminates the need for adding margins to compensate for tumour motion.[45]
When targeting LN levels as in the current workflow, however, the impact of the measured magnitude of motion of individual LNs to dose delivery will not be clinical significant because the LNs lie within the CTV levels and the PTV margin for a level is larger than the measured individual LN displacement. When aiming for individual LN irradiation without the MRI linac on the other hand, intrafraction motion management will be important. Without MRI it is not possible to directly track individual LNs. Therefore, as no beam steering or gating can be used, the uncertainties in LN position caused by intrafraction motion should then be incorporated in planning margins.
In the end, accurate motion tracking and compensation will ultimately lead to higher targeting accuracy. This will not only play a role in more precise target dosage, but will also contribute to normal tissue sparing.

4.5 Conclusion

In this chapter intrafraction displacement of individual LNs was quantified on cine MRI images. Maximum LN displacements in LR, SI, and AP direction ranging from 1.6–1.8 mm in five breast cancer patients and 1.7–2.1 mm in seven healthy volunteers were found. These displacements included LN movement due to breathing motion as well as baseline drifts. The impact of this motion on conventional RT to LN target levels is likely small. However, for future RT strategies aiming at individual LNs in a single or few fractions, this motion is relevant to consider because of long treatment times and small target volume. Potentially online target guidance strategies on the MRI linac could be used to compensate for the intrafraction motion and ensure safe dose delivery. Otherwise, and for RT treatment aimed at individual LNs on conventional linacs, adequate margins to prevent geometrical miss of the target have to be selected.

5 Contour propagation

5.1 Introduction

With the introduction of the MRI linac it becomes possible to perform high-quality daily imaging before and during treatment. Because of this, perfect optimization of the treatment to the anatomical situation of the day will be possible. Ideally, this will enable adaptive radiation therapy[61] to optimally account for geometric and anatomical changes.[62] This would allow for correction of interfraction anatomical variation that cannot simply be corrected by shift of the treatment couch. This is important when targets become smaller, margins are reduced, and high doses are delivered as is applied more and more hypofractionated schedules.[63]

To be able to perform adaptive plan optimization in an online setting, one of the necessary steps is the delineation of target volumes and organs at risk on the newly acquired scan of the day.[62,64] Starting contouring from scratch would be a time consuming job and takes too long for plan optimization in the online setting. Therefore, a solution would be to propagate the contours made on the images before treatment by using deformable image registration.

Several studies have investigated contour propagation for different treatment sites. These include prostate,[65,66] lung,[67] and head and neck.[68] However, contour propagation in these studies was based on CT imaging and not on MR imaging. For cervical cancer patients contour propagation has been investigated on MR images.[64] The researchers concluded that soft-tissue based deformable registration using MRI significantly improved registration accuracy compared to rigid registration on bony anatomy.[64] Another study also used contour propagation on MR images.[62] Here it was used for clinical application of online adaptive RT treatment for different treatment sites using the MRIdian System.[69] Unfortunately, no quantitative results of contour propagation quality were reported in this study. It is only mentioned that physicians were required to verify the contours of target and OARs and tools were available for manual modification. Until now, no investigation of contour propagation on MR images for individual LNs has been performed.

For the chapter on interfraction displacement analysis (chapter 3) manual delineations of individual LNs were already performed in two or three scans per patient in five patients. Here, these manually delineated contours were used for contour propagation and comparison with propagated contours. With these data, we carried out a first investigation of intrapatient contour propagation of individual LNs to explore potential application in online adaptive MRI-guided radiotherapy.

5.2 Methods and materials

Intrapatient contour propagation of individual lymph node delineations was tested using a commercial image registration package (ADMIRE Research, version 1.13.3, Elekta AB, Stockholm, Sweden). To evaluate the accuracy of the propagated delineations a comparison with manual delineations was performed.

5.2.1 Imaging data

Available data to test intrapatient contour propagation consisted of all acquired T1 mDIXON scans from the five TIMBRE patients. Image acquisition is described in chapter 2 Study population and

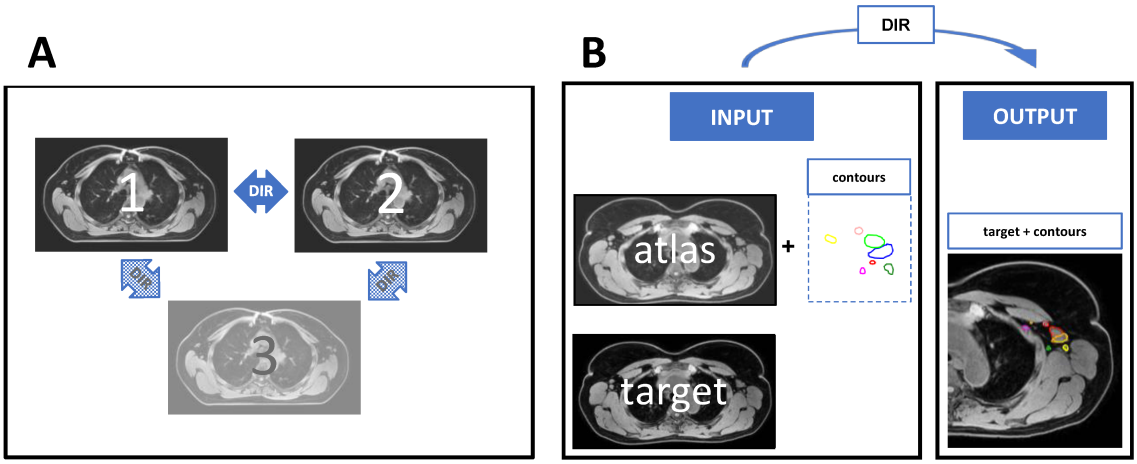

Figure 5.1: ***Intrapatient DIR combinations and DIR workflow.*** *A) all combinations of atlas and target sets that were tested for contour propagation. A third set was only available in two of five patients. B) Intrapatient contour propagation workflow. An atlas set with manually delineated LN contours and a target set to which the contours have to be propagated serve as input. DIR is performed with ADMIRE Research. A target set with propagated contours is produced as output.*

Abbreviations: DIR: deformable image registration.

MRI data. Only the water-only images were used to test intrapatient contour propagation. In total 12 T1 water-only images were available, two T1 scans each for three patients, and three T1 scans for the other two patients. On every scan individual lymph nodes were manually delineated (see chapter 3 Interfraction lymph node displacement).

5.2.2 Contour propagation

ADMIRE Research was used to perform the intrapatient contour propagation. The software uses a normalized mutual information algorithm to carry out deformable image registration (DIR) from one image to another. For each patient all sets served as atlas set (scan including delineations that have to be propagated) and target set (scan without delineation to which the LN delineations have to be propagated), see Figure 5.1A. The atlas set is deformed towards the target set and the LN delineations are deformed in the same way. This results in the propagated contours (Figure 5.1B).

5.2.3 Evaluation of contour propagation accuracy

To evaluate the accuracy, the propagated contours were compared to the manual delineations that were available for all image sets. For comparison of the contour outlines, the shortest distance of the propagated contour to the manual contour is calculated in each surface point. The mean of this distance is taken per LN and averaged over all LNs per patient using the an in-built evaluation tool of ADMIRE Research. The standard deviation (SD) over all LNs per patient is calculated from all mean distances. Furthermore, the difference in centre of gravity position (CoG) was also measured per LN to get an idea of the overall spatial accuracy of the propagated contours. This was performed in MATLAB R2015a (The Mathworks, Natick, MA).

5.2.4 Statistical analysis

To further compare the propagated contours to the manually delineated contours, the LN volumes were determined. This was performed using MATLAB R2015a (The Mathworks, Natick, MA). A Bland-Altman plot was calculated using GraphPad Prism 6.02 (GraphPad Software, Inc., La Jolla, California, USA) to show the difference between the volumes as a function of the average volume. In addition, a non-parametric Wilcoxon matched-pairs signed rank test was performed to statistically evaluate the volume differences. A p-value smaller than 0.05 was considered statistically significant.

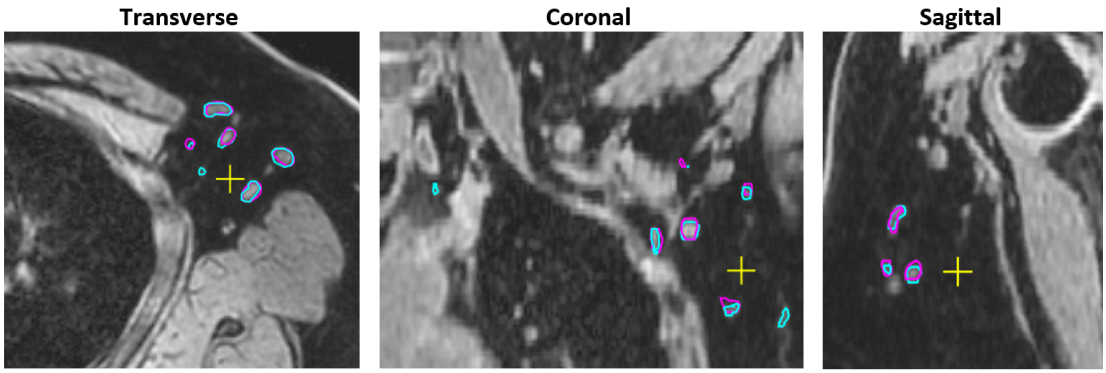

Figure 5.2: ***Example of propagated contours (pink) and manual contours (blue) in the same scan.*** *The yellow crosshair indicates the intersection of the orthogonal planes.*

5.3 Results

In 12 scans of five TIMBRE patients a total of 18 different intrapatient propagations could be performed. Six combinations for the two patients with 3 scan sets and two for the patients with 2 scan sets. Time necessary for contour propagation per case ranged from 31 to 50 seconds, and was on average 40 seconds. In Figure 5.2 an example of a scan with the manually delineated contours and the contours propagated from a different set of the same patients is shown. It is visible that in general the propagated contours are very similar to the manually delineated contours.

The mean distance between the propagated contours and the manual contours is shown in Table 5.1. For all tested combinations the average of the mean distances between manual and propagated contour was 0.70mm with a standard deviation of 0.30mm.

Median manual LN volume was 0.090 mL (range: 0.017 mL minimum − 2.2 mL maximum) and the median of the propagated LN contours volume was 0.079 mL (0.0079−2.2mL). This shows a median difference of -0.010mL, in which the median volume of the propagated contour is 11% smaller than the manual contour. The p-value of the Wilcoxon signed rank test was < 0.0001 which indicates that this difference in size was statistically significant. The differences in volumes represented as a function of the average are shown in Figure 5.3.

The distances between the centres of gravity are shown in Table 5.2. The overall mean distance between the centres of gravity is 1.09mm with an SD of 0.60mm. This is somewhat larger than the mean distances between the contours.

Table 5.1: ***Mean distances (SD) [mm] between propagated and manual LN contours.*** *Mean distances are shown for all possible atlas and target set combinations. SD are calculated for all separate LN mean distances per combination.*

TIMBRE ID	Target set	Atlas set	01	02	03	04	05	Total (n=5)
# LNs			18	23	36	18	27	**122**
Mean distance [mm] (SD)	1	2	0.58 (0.21)	0.63 (0.31)	0.94 (0.32)	0.50 (0.22)	0.51 (0.21)	
	1	3	0.76 (0.29)			0.44 (0.26)		
	2	1	0.74 (0.22)	0.79 (0.28)	0.77 (0.52)	0.64 (0.19)	0.68 (0.25)	
	2	3	0.82 (0.27)			0.72 (0.43)		
	3	1	0.82 (0.25)			0.55 (0.28)		
	3	2	0.90 (0.39)			0.55 (0.29)		
Mean	**All**	**All**	**0.77 (0.27)**	**0.71 (0.29)**	**0.86 (0.42)**	**0.57 (0.28)**	**0.59 (0.23)**	**0.70 (0.30)**

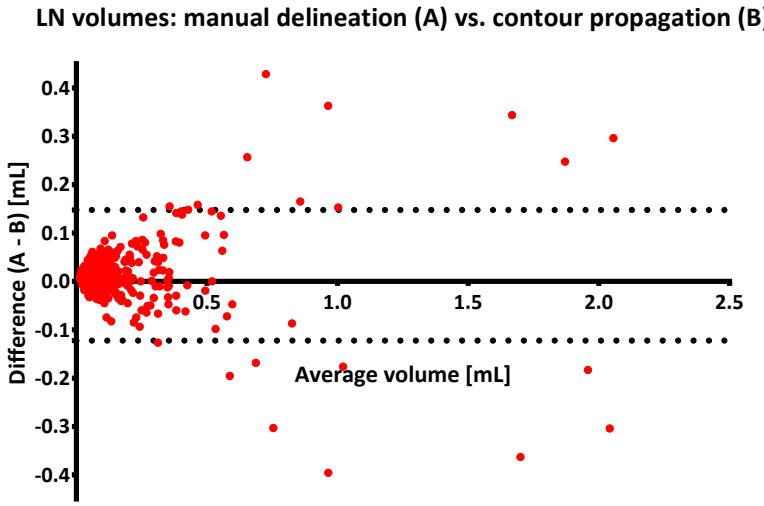

Figure 5.3: ***Bland-Altman plot of LN volumes.*** *The plot indicates the difference in LN volume between the manual and propagated contours plotted against the average of the two values. The dotted lines indicate the 95% limits of agreement. The Wilcoxon signed rank test gives a p-value of <0.0001 and indicates that propagated contours are statistically significant smaller than manual contours.*

5.4 Discussion

In this chapter we explored contour propagation for individual LN contours on MR images using deformable image registration. An overall mean distance (SD) of 0.70mm (0.30mm) between manual and propagated LN contours and a mean difference (SD) in centre of gravity position of 1.09mm (0.60mm) were found. These distances are small and may indicate that contour propagation might be a good start for individual LN delineation on a new scan of the same patient.

In addition, it was seen that the median propagated LN volumes were 11% smaller than the median manually delineation LN volumes. This suggests that we should not only pay attention to the geometrical correctness of the propagated contour, but also to its size.
The smaller LN volumes that were seen after propagation compared to the manual contours might be caused by resampling the propagated contours to the voxel grid of the new scan. Voxels belonging to the LN contour in the atlas image might be mapped outside voxels of the target scan. It is considered that this could explain the decrease in LN volume. The loss of volume could be corrected for by enlarging the LN contour with a predefined margin. Geometrical accuracy of the propagated contours is therefore more important than exactly identical LN volumes. To correct for the decrease

Table 5.2: ***Distance between centres of gravity [mm] of the manual and propagated contours.***

TIMBRE ID	Target set	Atlas set	01	02	03	04	05	Total (n=5)
# LNs			18	23	36	18	27	**122**
Mean distance [mm] (SD)	1	2	0.93 (0.41)	1.20 (0.79)	1.47 (0.71)	0.81 (0.42)	0.75 (0.37)	
	1	3	1.14 (0.59)			0.95 (0.53)		
	2	1	1.03 (0.49)	1.08 (0.60)	1.40 (0.79)	0.79 (0.46)	0.80 (0.55)	
	2	3	1.31 (0.72)			0.81 (0.63)		
	3	1	1.45 (0.54)			0.92 (0.58)		
	3	2	1.64 (0.67)			0.91 (0.52)		
Mean	**All**	**All**	**1.25 (0.57)**	**1.14 (0.70)**	**1.44 (0.75)**	**0.86 (0.52)**	**0.78 (0.46)**	**1.09 (0.60)**

in size it first has to be investigated if loss of LN voxels is isotropically distributed around the LN contour or if correction has to be carried out only in certain directions.

As mentioned in the introduction, no other studies previously investigated contour propagation for individual LNs. It is therefore not possible to compare the accuracy of our results to outcomes of other studies. To get an idea of the level of accuracy of the contour propagation, it would be helpful to study inter- and intraobserver variation of individual LN delineation. This could show which level of accuracy the propagated contours have in comparison to the inter- and intraobserver agreement. This would indicate how reliable the contour propagation is without any manual modification. Currently no data on the interobserver agreement for individual LNs are available. A study by Ciardo et al.[70] has recently investigated interobserver variability in the delineation of LN levels between different observers from different institutes, following delineation guidelines. They reported a moderate agreement based on an overall median Dice similarity coefficient of 0.66. Furthermore, they also reported a CoG distance. For levels 1 to 4 this ranged from 0.5 $\pm$ 0.5mm (median $\pm$ interquartile range) to 0.7 $\pm$ 0.9mm.[70] These CoG distances are slightly lower than the CoG distances we found for the propagated contours. This could indicate that the accuracy of the propagated LN contours is lower than the accuracy of manual delineation in the presence of interobserver variation. However, it is not clear whether this measured interobserver agreement in the delineation of LN levels can be translated into a comparable agreement in the delineation of individual LNs. Therefore, this would be an interesting topic for further research. Interobserver variation in delineation of tumour positive LNs will be investigated in the TIMBRE patient study.[31]

Besides this, it would also be interesting to evaluate the accuracy of a propagated contour plus a CTV or PTV margin. This could be a topic of further research. When a propagated contour in combination with a PTV margin could provide comparable individual lymph node GTV/CTV dose coverage as a manual delineation plus PTV margin this could reduce level of manual interaction that will be necessary in recontouring.

Furthermore, we could evaluate the value of contour propagation for organs at risk and LN level CTVs on MRI. For online adaptive radiotherapy, not only target GTV delineations should be accurately adapted to the anatomy of the day, also all other relevant structures have to be checked. This could also be conducted in future research.

In the interfraction displacement analyses (see chapter 3 Interfraction lymph node displacement) it was seen that displacement distances were different for individual LNs in the same patient. Therefore, a translational correction, which can be made with the treatment couch, or even a rigid registration also taking rotations into account, are not sufficient to adequately adapt for the different displacements of all individual LNs together.[63] This showed that contour adaptation of individual LNs in the new scan is necessary. It is interesting to see that the distances between CoGs of the propagated and manual contours found in this chapter were smaller than the measured interfraction displacement of individual LNs. This indicates that the deformable image registration used for the contour propagation is better able to handle the independent motion of individual LNs, as we expected. Furthermore, this demonstrates the value of online contour adaptation before treatment.

In our investigation contour propagation took on average 40s. Although it was not tested, it is expected that time of contour propagation together with time needed for manual correction of the contours is much less than starting manual contouring on the new scan from scratch. Therefore, it will be helpful in saving time necessary for delineation of the new scan. Fast delineation of contours is essential when aiming for plan adaptation in the online setting.

Eventually contour propagation can be used for fast contouring of a new daily scan of a patient. This is necessary when aiming for an online adaptive treatment on the MRI linac to fully optimize the irradiation based on the anatomy of the day. The method should be tested in a larger patient population and can be tested for OAR contour propagation. It still has to be evaluated how much user input is necessary for manual correction of the propagated contours. Total time necessary for

contour propagation, verification by the physician and correction has to be determined. This will show if application in the online adaptive setting is feasible. Contours on the scan of the day can then be used to evaluate if the beforehand prepared treatment plan constraints are met or if an online plan reoptimization has to be performed. The new contours can also be used in this reoptimization step if plan optimization in necessary.
Additionally, contour propagation will be helpful in extending the interfraction motion analyses to more patients. Only the first scan has to be contoured from scratch. Contour propagation can be used to create initial delineations of all contours on the other scan sets of the same patients. Analogous to contour propagation for online adaptive RT treatment this will save a lot of time in delineating all LNs.

5.5 Conclusion

This chapter showed a first exploration of the convenience of contour propagation for individual LN delineation. Deformable image registration with a commercial software package was used to propagate the contours. Differences in the outlines of the propagated contour compared to the manual contour were on average 0.70mm and the average distance between the centres of gravity was 1.09mm. Overall the propagated contours gave a good initial delineation of the LNs. With manual adaptations this will give good delineation results while saving time compared to delineating from scratch. Therefore, it is recommended to further investigate the propagation results in more patients and to also examine its applicability for CTV/PTV and OAR contour propagation. Before using it in an adaptive RT workflow with the MRI linac it has to be tested if the method combined with necessary manual adaptations by a physician are fast enough for online application.

6 Patient comfort

To assess patient comfort and patient experiences during the scanning session, each patient was asked to fill in an evaluation form afterwards. Answers to these questions give an indication if the position and duration to lie in the scanning position are agreeable from patient experience and if there are things that have to be adapted in the future process towards clinical application.

It was important to evaluate this because the MRI scanning takes longer than the current CT scanning and RT treatment session duration. Furthermore, in future treatment with daily adaptable plan optimization possibilities of the MRI linac, the duration that the patient is lying in RT treatment position might be considerably longer than during conventional irradiation treatment. In addition, patients have to lie inside the tunnel bore of the MRI instead of the shorter bore of the CT scanner, which can influence the experience during scanning. Therefore, it is helpful to collect patient feedback and experiences.

6.1 Evaluation form

The questionnaire (originally in Dutch) consisted of four different questions:

From the following topics, what was your experience **during** the MRI session?

	No, not at all	Yes, somewhat	Yes, fairly	Yes, very much
1. I experienced the MRI session as painful.	☐	☐	☐	☐
2. I experienced the MRI session as uncomfortable.	☐	☐	☐	☐
3. I was afraid during the MRI session.	☐	☐	☐	☐
4. Have you experienced any physical (health) complaints during the MRI session?				
☐ No → end of questionnaire				
☐ Yes → give a short description:				

6.2 Results

The experiences reported by the 5 TIMBRE patients are shown in Table 6.1.

No severe painful, uncomfortable or anxious experiences were reported during the MRI scanning sessions. However, 4 out of 5 patients reported a form of physical (health) complaints. These could be mainly addressed to soreness or stiffness due to maintaining the same position and having to lie still during a scan set.

Table 6.1: *Results from the evaluation forms on experiences during the MRI session.*

	No, not at all	Yes, somewhat	Yes, fairly	Yes, very much
1. I experienced the MRI session as painful.	60%	40%	0%	0%
2. I experienced the MRI session as uncomfortable.	60%	40%	0%	0%
3. I was afraid during the MRI session.	80%	20%	0%	0%
4. Have you experienced any physical (health) complaints during the MRI session?				
20% No				
80% Yes*				

* Short descriptions of complaints: a bit sensitive head and neck, back muscles, neck muscles, cold and numb arms, pressure spots on shoulders and tail bone, right arm and shoulder

6.3 Discussion

No severe negative experiences during the MRI scanning session were reported. However, 4 out of 5 patients reported some type of physical complaints. This can indicate that in general the procedure is well endured, although all patients except one experienced light discomfort.

Since the protocol was not fully optimized when scanning these first five patients some protocol tuning was performed during all scanning sessions. Therefore, time spent on the scanner table was longer than initially aimed for. It was not exactly measured, but some patients had to lie for up to 35 minutes in treatment position during a single scan set, including patient set up and MRI scanning. In addition, the full scanning protocol with three scanning blocks (scanned in patient 01 and 04) proved to be too long for the available time slot per patient. After these five patients the protocol was adapted to shorten the scanning time.

From verbal feedback received from patients after scanning, we heard that all physical complaints disappeared soon after leaving the scanner table.

With the adapted scanning protocol it is expected that future TIMBRE study patients can endure the scanning session well. For future MRI linac treatment it is recommended to try to keep the patient in the RT treatment position as short as possible. It is not yet known how an MRI linac treatment workflow for LN irradiation will look like and how much time it will take. Therefore, it has still to be investigated if patient can maintain treatment position long enough for a complete online adaptive treatment session.

Moreover, all TIMBRE patients were scanned prior to surgery. Therefore, it is also not known how long patients are able to sustain this position after sentinel lymph node biopsy. However, in a previous research it was found that SNB did not affect posture endurance,[27] therefore no major problems in posture endurance are expected. Nevertheless, breast-conserving surgery or mastectomy can also lead to pain in the flank or chest wall, i.e. caused by oedema or seroma. This can impede comfortably retaining the scanning position. Therefore, pre-operative scan acquisition would be most optimal.

7 General discussion and conclusion

7.1 Summary

In this masters thesis I explored MRI-guided radiation therapy of regional lymph nodes in breast cancer patients.

Organ or patient motion on different time scales can lead to errors regarding the geometrical accuracy of the RT treatment. It is therefore important to identify and quantify the motion to be able to minimize the error sources and take them into account in the treatment workflow. Potential errors caused by organ motion can be included for instance in the treatment plan preparation phase by using margins or can ultimately be completely eliminated with real-time motion tracking on the MRI linac.
First, *inter*fraction displacement of individual lymph nodes was investigated in **chapter 3**. It was seen that after local rigid, displacements of individual lymph nodes up to 2.5mm were present. Displacements differed between lymph nodes in different lymph node levels. Furthermore, displacement amplitude depended on the choice of the registration area.
Next, the intrafraction displacements of individual lymph nodes were assessed in **chapter 4**. In 1 minute cine MRIs displacements of individual lymph nodes were tracked. The motion pattern showed that lymph nodes moved due to breathing motion. The mean maximum displacement amplitudes in left-right, superior-inferior and anterior-posterior direction were between 1.6mm and 2.1mm.

The measured interfraction displacements were small. However, the analyses showed that the individual lymph nodes moved independently. Therefore, patient set-up correction with the treatment couch cannot correct for the interfraction displacements of all LNs simultaneously. This indicates that only online adaptive treatment with daily imaging and recontouring prior to treatment can perfectly correct for the displacements. Otherwise, the independent motion of the individual LNs has to be incorporated in PTV margins.
Contour propagation of individual lymph node delineations with deformable image registration between two scans of the same patient was explored as potential strategy for online recontouring (**chapter 5**). Average distance between the boundaries of the propagated contours and the manual delineations in the same scan was 0.70mm. The distance between the centres of gravity of the manual and propagated contours (1.1mm) was smaller than the interfraction displacements (1.6-2.5mm). This indicates that the deformable image registration takes into account the independent movements of the separate lymph nodes, as was expected. Propagated LN contours still have to be verified and when necessary manually adapted by a physician. It has yet to be investigated if this can be performed fast enough for online plan adaptation.

Because regional lymph node irradiation on the MRI linac will probably take longer than conventional breast and regional lymph node RT treatment in the same position, it was important to evaluate if patients can comfortably maintain the treatment position. Therefore, all TIMBRE patients filled in an evaluation form at the end of the MRI scanning session (**chapter 6**). These showed that in general the patients can well sustain the position. However, 4 out of 5 TIMBRE patients reported about a somewhat painful or uncomfortable physical complaint. These could all be explained by lying still in the same position for a long time. All patients orally reported that the discomfort decreased immediately after leaving the scanner table.

The above mentioned results can help in developing a workflow for regional lymph node irradiation on the MRI linac. Furthermore, they indicate the level of motion that has to be taken into account in uncertainty margins when combining MRI with conventional CT for target definition.

7.2 Recommendations for future research

Although several topics necessary for workflow development of MRI-guided regional lymph node irradiation were investigated in this thesis, others still have to be studied.

Conventional locoregional breast RT is aimed at LN levels, usually level 1-2 or level 1-4, and therefore targets all LNs inside the levels. When targeting individual LNs it has to be separately determined which LNs should be irradiated. Furthermore, by irradiating LN levels, also the vessels of the lymphatic system between all the LNs receive a high dose. It should also be determined if and how much dose these lymphatic vessels should receive. Different options can be considered.
One possibility would be to keep irradiating the LN levels, but with a lower total dose (on a conventional linac). This would reduce the dose to the surrounding organs at risk and potentially reduce treatment-induced toxicity. The individual LNs can be sequentially irradiated on the MRI linac to the regular total dose. This option could be used only for cN0 patients with limited disease in the sentinel LNs. Feasibility studies are required to assess if a lower dose to the lymph vessels can be technically achieved and to evaluate if it is clinically safe in terms of local disease control. Eventually, such a treatment might be given completely on the MRI linac when a large field length can be irradiated, provided that the ERE does not pose any problems in the dose distribution.
Another option would be to only replace the sequential 8-10 fraction boost treatments targeted at positive LNs with a single fraction ablative dose boost on the MRI linac.[28] This boost treatment is indicated for patients with LNs that remain tumour-positive after neoadjuvant chemotherapy. Using a single fraction boost would reduce the number of treatment fractions without increasing the dose to the OARs. At first, this approach could be adopted by adding MRI guidance to the CT workflow. Eventually, this treatment can be given on the MRI linac. With the online image guidance capabilities of the MRI linac, the necessary treatment margins might even be reduced compared to current boost margins, which would lead to even more normal tissue sparing.
However, these kind of approaches lead to two more unaddressed topics. When it is desired to only target individual tumour positive lymph nodes, it has to be determined which LNs this are. Moreover, treatment margins for individual LN targeting, with or without online MRI guidance have to be determined.

The MRI scans used for this study are optimized for LN visualization and anatomical information, not for LN staging.[26] Therefore, other methods are required for detection of tumour positive LNs. LN staging could be performed before treatment and image registration could be used to identify the LNs of interest from the pre-treatment MRI also on the MRI linac. The most promising results in terms of sensitivity and specificity for detection of LN metastasis have been reported for USPIO-enhanced MRI.[24,25] The results of these MRI techniques have to be confirmed in larger studies and also application for individual node assessment has to be investigated.[24] Another option for detection of nodal metastases would be the use of positron emission tomography (PET). High specificity is reported, but lower sensitivity[71] compared to MRI.
In current clinical practice PET is used for LN staging. Because PET is necessary for identification of tumour-positive LNs, the combination of MRI imaging, PET-CT and RT planning CT for delineation of positive lymph nodes is currently under investigation in the TIMBRE study. In the future, a PET-MRI scanner will also be available in the UMC Utrecht.

The interfraction and intrafraction displacements of the anatomy with respect to the reference scan on which the treatment plan is simulated may lead to geometrical errors in dose delivery. With online image guidance the influence of the errors can be reduced. However, some uncertainty will always remain, especially when real-time target tracking is not yet possible or when no daily MRI imaging is available when using conventional linacs. As long as no perfect correction for the positional errors is possible, the geometric uncertainties have to be incorporated in the planning process by adding a PTV margin.[33] Several suggestions have been done how to calculate the necessary margin. One widely used margin recipe is from Van Herk.[33] The margin is calculated using the SD of

the random error, σ, and the SD of the systematic error, Σ:

$$margin = 2.5\Sigma + 0.7\sigma. \tag{7.1}$$

It is further suggested that respiration motion with a peak-to-peak amplitude (A) smaller than 1 cm (as we observed in chapter 4 Intrafraction lymph node displacement) can be treated the same as random errors, for which the SD of respiration motion can be calculated as $0.358A$.[72] Inter- and intrafraction components of the systematic and random errors can be combined using $\Sigma = \sqrt{\Sigma_{inter}^2 + \Sigma_{intra}^2}$ and $\sigma = \sqrt{\sigma_{inter}^2 + \sigma_{intra}^2}$.[73,74]

Not enough data were available to calculate margins from the measured inter- and intrafraction displacements. With more different patients and at least three scans per patient to determine a mean interfraction displacement per patient, the margin recipes could be used. Therefore, this topic can be evaluated in the continuation of the TIMBRE study.

In order to perform online adaptive radiotherapy to account for inter- and intrafraction anatomy changes, not only daily imaging and recontouring of organs is necessary, also online treatment plan adaptation is necessary.[23] This is a topic that is currently investigated.[75–77] Evaluation of such methods to the application of individual LN irradiation would be an interesting subject for further research. Furthermore, a dosimetric comparison of online adaptive replanning and the use of a plan without online replanning but with the calculated necessary margins would also be interesting. With online MRI guidance for patient set-up the necessary margins can possibly already be reduced compared to conventional set-up, which will improve organ at risk sparing.

Currently, registered CT data are necessary for the pre-treatment dose calculations. The use of the combination of MRI and CT involves a registration step and transferring of contours. This can lead to a registration error that influences treatment accuracy. By omitting the CT and using only MRI images for delineation as well as treatment planning, the potential errors in the registration step are removed. However, for MRI-only treatment planning it is necessary to generate a synthetic CT since MRI does not inherently contain electron density information. Synthetic CT generation already is a topic of active research.[78,79] Application of methods for synthetic CT generation and accuracy of dose calculations for MRI-only treatment planning for regional RT in breast cancer patients is another topic that has to be investigated in future research.

7.3 Conclusion

The investigation of MRI guidance for individual LN irradiation in breast cancer patients is a novel step towards a highly accurate, minimal invasive treatment approach for regional LNs. The greatest improvement with this approach is a potential reduction in treatment-induced toxicity. For the future application of MRI guidance, inter- and intrafraction displacement of individual LNs were investigated in this thesis, as well as contour propagation for online adaptive RT and the patient comfort. The results of these investigations are valuable for workflow development for MRI-guided individual LN irradiation. The outcomes will help in making use of the advantages of MRI added to the conventional CT-based workflow as well as making use of the possibilities of the MRI linac. Both approaches will facilitate improvement in the accuracy of regional LN irradiation. This will lead to optimal target coverage, improved normal tissue sparing and a reduction in treatment-induced toxicity. The first step in treatment innovation will be the addition of MRI to the conventional workflow. Ultimately, the MRI linac will present a safe and efficient minimally invasive approach of regional LN treatment in breast cancer patients. Ideally, the MRI-guided RT treatment can eventually completely replace axillary surgery.

References

[1] Nederlandse Kankerregistratie, beheerd door IKNL ©. www.cijfersoverkanker.nl. Online; accessed 1 October 2016.

[2] Mammacarcinoom, Landelijke richtlijn, Versie: 2.0. www.onconline.nl, 2012.

[3] Van de Velde, C. J. H., Nortier, J. W. R., Elkhuizen, P. H. M., van Diest, P. J., and Zonderland, H. M. Hoofdstuk 24: Mammatumoren. In *Oncologie*, chapter 24, pages 431–452. Bohn Stafleu van Loghum, Houten, achtste edition, 2011.

[4] Wong, S. L., Chao, C., Edwards, M. J., et al. Accuracy of sentinel lymph node biopsy for patients with T2 and T3 breast cancers. *The American Surgeon*, 67:522–526, 2001.

[5] Hunt, K. K., Robb, G. L., Strom, E. A., Ueno, N. T., Buzdar, A. U., and Freedman, R. S. *Breast Cancer, 2nd edition*. Springer, 2008.

[6] de Jongh, T. O. H., Buis, J., Daelmans, H. E. M., et al. *Fysische diagnostiek*. Bohn Stafleu van Loghum, 2010.

[7] Lucci, A., McCall, L. M., Beitsch, P. D., et al. Surgical complications associated with sentinel lymph node dissection (SLND) plus axillary lymph node dissection compared with SLND alone in the American College of Surgeons Oncology Group trial Z0011. *Journal of Clinical Oncology*, 25(24):3657–3663, 2007.

[8] Fleissig, A., Fallowfield, L. J., Langridge, C. I., et al. Post-operative arm morbidity and quality of life. Results of the ALMANAC randomised trial comparing sentinel node biopsy with standard axillary treatment in the management of patients with early breast cancer. *Breast Cancer Research and Treatment*, 95(3):279–293, 2006.

[9] Hayes, S. C., Janda, M., Cornish, B., Battistutta, D., and Newman, B. Lymphedema after breast cancer: Incidence, risk factors, and effect on upper body function. *Journal of Clinical Oncology*, 26(21):3536–3542, 2008.

[10] DiSipio, T., Rye, S., Newman, B., and Hayes, S. Incidence of unilateral arm lymphoedema after breast cancer: A systematic review and meta-analysis. *The Lancet Oncology*, 14(6):500–515, 2013.

[11] Giuliano, A. E., McCall, L., Beitsch, P., et al. Locoregional Recurrence After Sentinel Lymph Node Dissection With or Without Axillary Dissection in Patients With Sentinel Lymph Node Metastases: The American College of Surgeons Oncology Group Z0011 Randomized Trial. *Annals of Surgery*, 252(3):426–433, 2010.

[12] Galimberti, V., Cole, B. F., Zurrida, S., et al. Axillary dissection versus no axillary dissection in patients with sentinel-node micrometastases (IBCSG 23-01): a phase 3 randomised controlled trial. *The Lancet Oncology*, 14(4):297–305, 2013.

[13] Donker, M., van Tienhoven, G., Straver, M. E., et al. Radiotherapy or surgery of the axilla after a positive sentinel node in breast cancer (EORTC 10981-22023 AMAROS): a randomised, multicentre, open-label, phase 3 non-inferiority trial. *Lancet Oncol*, 15(12):1303–1310, 2014.

[14] Bundred, N. J., Barnes, N. L. P., Rutgers, E., and Donker, M. Is axillary lymph node clearance required in node-positive breast cancer? *Nature Reviews Clinical Oncology*, 12(1):55–61, 2015.

[15] Whelan, T. J., Olivotto, I. A., Parulekar, W. R., et al. Regional Nodal Irradiation in Early-Stage Breast Cancer. *The New England Journal of Medicine*, 373(4):307–16, 2015.

[16] Poortmans, P. M., Collette, S., Kirkove, C., et al. Internal Mammary and Medial Supraclavicular Irradiation in Breast Cancer. *New England Journal of Medicine*, 373(4):317–327, 2015.

[17] Offersen, B. V., Boersma, L. J., Kirkove, C., et al. ESTRO consensus guideline on target volume delineation for elective radiation therapy of early stage breast cancer. *Radiotherapy and Oncology*, 114(1):3–10, 2015.

[18] Sanuki, N., Takeda, A., Amemiya, A., et al. Outcomes of Clinically Node-Negative Breast Cancer Without Axillary Dissection: Can Preserved Axilla Be Safely Treated with Radiation after a Positive Sentinel Node Biopsy? *Clinical Breast Cancer*, 13(1):69–76, 2013.

[19] Hoebers, F. J. P., Borger, J. H., Hart, A. A. M., Peterse, J. L., Rutgers, E. J. T., and Lebesque, J. V. Primary axillary radiotherapy as axillary treatment in breast-conserving therapy for patients with breast carcinoma and clinically negative axillary lymph nodes. *Cancer*, 88(7):1633–1642, 2000.

[20] Leer, J. W. H., Van der Kogel, A. J., and Huizenga, H. Hoofdstuk 7: De rol van radiotherapie bij de behandeling van kanker. In *Oncologie*, chapter 7, pages 165–174. Bohn Stafleu van Loghum, Houten, achtste edition, 2011.

[21] Raaymakers, B. W., Lagendijk, J. J. W., Overweg, J., et al. Integrating a 1.5 T MRI scanner with a 6 MV accelerator: proof of concept. *Physics in Medicine and Biology*, 54(12):N229–N237, 2009.

[22] Lagendijk, J. J. W., Raaymakers, B. W., and van Vulpen, M. The Magnetic Resonance Imaging-Linac System. *Seminars in Radiation Oncology*, 24(3):207–209, 2014.

[23] Lagendijk, J. J. W., van Vulpen, M., and Raaymakers, B. W. The development of the MRI linac system for online MRI-guided radiotherapy: a clinical update. *Journal of Internal Medicine*, 280(2):203–208, 2016.

[24] Kuijs, V. J. L., Moossdorff, M., Schipper, R. J., et al. The role of MRI in axillary lymph node imaging in breast cancer patients: a systematic review. *Insights Imaging*, 6(2):203–215, 2015.

[25] Harnan, S. E., Cooper, K. L., Meng, Y., et al. Magnetic resonance for assessment of axillary lymph node status in early breast cancer: A systematic review and meta-analysis. *European Journal of Surgical Oncology*, 37(11):928–936, 2011.

[26] Van Heijst, T. C. F., Van Asselen, B., Pijnappel, R. M., et al. MRI sequences for the detection of individual lymph nodes in regional breast radiotherapy planning. *British Journal of Radiology*, 89:20160072, 2016.

[27] Van Heijst, T. C. F., Eschbach-Zandbergen, D., Hoekstra, N., et al. Supine MRI for regional breast radiotherapy: imaging axillary lymph nodes before and after sentinel-node biopsy. *Phys Med Biol [in press]*, 2017.

[28] Van Heijst, T. C. F., Hoekstra, N., Philippens, M. E. P., et al. *MRI-guided single-fraction boost delivery on individual axillary lymph nodes [PhD Thesis Chapter 6 - Manuscript in preparation]*. PhD thesis, University of Utrecht, 2017.

[29] Van Heijst, T. C. F., den Hartogh, M. D., Lagendijk, J. J. W., van den Bongard, H. J. G. D., and van Asselen, B. MR-guided breast radiotherapy: feasibility and magnetic-field impact on skin dose. *Physics in medicine and biology*, 58(17):5917–30, 2013.

[30] Kontaxis, C., Bol, G. H., Lagendijk, J. J. W., and Raaymakers, B. W. Towards adaptive IMRT sequencing for the MR-linac. *Physics in medicine and biology*, 60:2493–2509, 2015.

[31] Charaghvandi, K. R., Gregorowitsch, M. L., Van Heijst, T. C. F., et al. Towards implementation of on-line MRI-guided radiation therapy in breast cancer patients - TIMBRE study - [METC protocol], 2016.

[32] Michalski, A., Atyeo, J., Cox, J., and Rinks, M. Inter- and intra-fraction motion during radiation therapy to the whole breast in the supine position : A systematic review. *Journal of Medical Imaging and Radiation Oncology*, 56:499–509, 2012.

[33] van Herk, M. Errors and Margins in Radiotherapy. *Seminars in Radiation Oncology*, 14(1):52–64, 2004.

[34] Hurkmans, C. W., Remeijer, P., Lebesque, J. V., and Mijnheer, B. J. Set-up verification using portal imaging; review of current clinical practice. *Radiotherapy and Oncology*, 58(2):105–120, 2001.

[35] Lagendijk, J. J. W., Raaymakers, B. W., den Berg, C. A. T. V., Moerland, M. A., Philippens, M. E., and van Vulpen, M. MR guidance in radiotherapy. *Physics in Medicine and Biology*, 59(21):R349–R369, 2014.

[36] Bol, G. H., Kotte, A. N. T. J., van der Heide, U. A., and Lagendijk, J. J. W. Simultaneous multi-modality ROI delineation in clinical practice. *Computer Methods and Programs in Biomedicine*, 6:133–140, 2009.

[37] Laaksomaa, M., Kapanen, M., Skyttä, T., Peltola, S., Hyödynmaa, S., and Kellokumpu-Lehtinen, P. L. Estimation of optimal matching position for orthogonal kV setup images and minimal setup margins in radiotherapy of whole breast and lymph node areas. *Reports of Practical Oncology and Radiotherapy*, 19(6):369–375, 2014.

[38] Laaksomaa, M., Kapanen, M., Haltamo, M., et al. Determination of the optimal matching position for setup images and minimal setup margins in adjuvant radiotherapy of breast and lymph nodes treated in voluntary deep inhalation breath-hold. *Radiation oncology*, 10:76, 2015.

[39] Juhler-Nøttrup, T., Korreman, S. S., Pedersen, A. N., et al. Interfractional changes in tumour volume and position during entire radiotherapy courses for lung cancer with respiratory gating and image guidance. *Acta oncologica*, 47(7):1406–1413, 2008.

[40] Weiss, E., Robertson, S. P., Mukhopadhyay, N., and Hugo, G. D. Tumor, lymph node, and lymph node-to-tumor displacements over a radiotherapy series: Analysis of inter- and intrafraction variations using active breathing control (ABC) in lung cancer. *International Journal of Radiation Oncology Biology Physics*, 82(4):e638–e645, 2012.

[41] Thomas, J. G., Kashani, R., Balter, J. M., Tatro, D., Kong, F.-M., and Pan, C. C. Intra- and inter-fraction mediastinal nodal region motion: implications for internal target volume expansions. *Med Dosim*, 34(2):133–139, 2009.

[42] Dijkema, I. M., Hofman, P., Raaijmakers, C. P. J., Lagendijk, J. J., Battermann, J. J., and Hillen, B. Loco-regional conformal radiotherapy of the breast: delineation of the regional lymph node clinical target volumes in treatment position. *Radiotherapy and Oncology*, 71:287–295, 2004.

[43] Josipovic, M., Persson, G. F., Logadottir, Á., Smulders, B., Westmann, G., and Bangsgaard, J. P. Translational and rotational intra- and inter- fractional errors in patient and target position during a short course of frameless stereotactic body radiotherapy. *Acta Oncologica*, 51(5):610–617, 2012.

[44] Qi, X. S., White, J., Rabinovitch, R., et al. Respiratory organ motion and dosimetric impact on breast and nodal irradiation. *International Journal of Radiation Oncology Biology Physics*, 78(2):609–617, 2010.

[45] Keall, P. J., Mageras, G. S., Balter, J. M., et al. The management of respiratory motion in radiation oncology report of AAPM Task Group 76. *Medical physics*, 33(10):3874–3900, 2006.

[46] Kleijnen, J.-P. J. E., van Asselen, B., Burbach, J. P. M., et al. Evolution of motion uncertainty in rectal cancer: implications for adaptive radiotherapy. *Physics in Medicine and Biology*, 61(1):1–11, 2016.

[47] Bjerre, T., Crijns, S., af Rosenschöld, P. M., et al. Three-dimensional MRI-linac intra-fraction guidance using multiple orthogonal cine-MRI planes. *Physics in Medicine and Biology*, 58:4943–4950, 2013.

[48] Seregni, M., Paganelli, C., Lee, D., et al. Motion prediction in MRI-guided radiotherapy based on interleaved orthogonal cine-MRI. *Physics in medicine and biology*, 61(2):872–87, 2016.

[49] Dowling, J., Dang, K., Fox, C. D., et al. Fast cine-magnetic resonance imaging point tracking for prostate cancer radiation therapy planning. *Journal of Physics: Conference Series*, 489:012027, 2014.

[50] Stemkens, B., Tijssen, R. H. N., de Senneville, B. D., et al. Optimizing 4-dimensional magnetic resonance imaging data sampling for respiratory motion analysis of pancreatic tumors. *International Journal of Radiation Oncology Biology Physics*, 91(3):571–578, 2015.

[51] Zachiu, C., Papadakis, N., Ries, M., Moonen, C., and Denis de Senneville, B. An improved optical flow tracking technique for real-time MR-guided beam therapies in moving organs. *Physics in Medicine and Biology*, 60(23):9003–9029, 2015.

[52] Zachiu, C., Denis de Senneville, B., Moonen, C., and Ries, M. A framework for the correction of slow physiological drifts during MR-guided HIFU therapies: Proof of concept. *Medical Physics*, 42(7):4137–4148, 2015.

[53] Wang, Z., Bovik, A., Sheikh, H., and Simmoncelli, E. Image quality assessment: form error visibility to structural similarity. *IEEE Transactions on Image Processing*, 13(4):600–612, 2004.

[54] Moran, J. M., Balter, J. M., Ben-David, M. A., Marsh, R. B., van Herk, M., and Pierce, L. J. The short-term displacement and reproducibility of the breast and nodal targets under active breathing control. *International Journal of Radiation Oncology Biology Physics*, 68(2):541–546, 2007.

[55] Jensen, C. A., Acosta Roa, A. M., Lund, J.-Å., and Frengen, J. Intrafractional baseline drift during free breathing breast cancer radiation therapy. *Acta Oncologica*, 56(6):867–873, 2017.

[56] Shannon, C. E. Communication in the presence of noise. *Proceedings of the IEEE*, 86(2):447–457, 1998.

[57] Denis de Senneville, B., Mougenot, C., and Moonen, C. T. W. Real-Time Adaptive Methods for Treatment of Mobile Organs by MRI-Controlled High-Intensity Focused Ultrasound. *Magnetic Resonance in Medicine*, 330(57):319–330, 2007.

[58] Brix, L., Ringgaard, S., Sorensen, T. S., and Poulsen, P. R. Three-dimensional liver motion tracking using real-time two-dimensional MRI. *Med Phys*, 41(4):042302, 2014.

[59] Glitzner, M., Fast, M. F., Denis de Senneville, B., et al. Real-time auto-adaptive margin generation for MLC-tracked radiotherapy. *Physics in Medicine and Biology*, 62(1):186–201, 2017.

[60] Crijns, S. P. M., Raaymakers, B. W., and Lagendijk, J. J. W. Proof of concept of MRI-guided tracked radiation delivery: tracking one-dimensional motion. *Physics in medicine and biology*, 57(23):7863–7872, 2012.

[61] Yan, D., Vicini, F., Wong, J., and Martinez, A. Adaptive radiation therapy. *Phys. Med. Biol*, 42:123–132, 1997.

[62] Acharya, S., Fischer-Valuck, B. W., Kashani, R., et al. Online Magnetic Resonance Image Guided Adaptive Radiation Therapy: First Clinical Applications. *International Journal of Radiation Oncology Biology Physics*, 94(2):394–403, 2016.

[63] Kupelian, P. and Sonke, J.-J. Magnetic Resonance-Guided Adaptive Radiotherapy: A Solution to the Future. *Seminars in Radiation Oncology*, 24(3):227–232, 2014.

[64] van der Put, R. W., Kerkhof, E. M., Raaymakers, B. W., Jürgenliemk-Schulz, I. M., and Lagendijk, J. J. W. Contour propagation in MRI-guided radiotherapy treatment of cervical cancer: the accuracy of rigid, non-rigid and semi-automatic registrations. *Physics in medicine and biology*, 54(23):7135–7150, 2009.

[65] Thornqvist, S., Petersen, J. B. B., Hoyer, M., Bentzen, L. N., and Muren, L. P. Propagation of target and organ at risk contours in radiotherapy of prostate cancer using deformable image registration. *Acta Oncol*, 49(7):1023–1032, 2010.

[66] Thor, M., Petersen, J. B. B., Bentzen, L., Høyer, M., and Muren, L. P. Deformable image registration for contour propagation from CT to cone-beam CT scans in radiotherapy of prostate cancer. *Acta oncologica*, 50:918–925, 2011.

[67] Hardcastle, N., van Elmpt, W., De Ruysscher, D., Bzdusek, K., and Tomé, W. A. Accuracy of deformable image registration for contour propagation in adaptive lung radiotherapy. *Radiation Oncology*, 8:243, 2013.

[68] Yeap, P. L., Noble, D. J., Harrison, K., et al. Automatic contour propagation using deformable image registration to determine delivered dose to spinal cord in head-and-neck cancer radiotherapy. *Physics in Medicine and Biology*, 62:6062–6073, 2017.

[69] Viewray. True Image Guided Radiation Therapy - The MRIdian System. `http://www.viewray.com/product`, 2017. Online; accessed 9 August 2017.

[70] Ciardo, D., Argenone, A., Boboc, G. I., et al. Variability in axillary lymph node delineation for breast cancer radiotherapy in presence of guidelines on a multi-institutional platform. *Acta Oncologica*, 56(8):1081–1088, 2017.

[71] Cooper, K. L., Meng, Y., Harnan, S., et al. Positron emission tomography (PET) and magnetic resonance imaging (MRI) for the assessment of axillary lymph node metastases in early breast cancer: systematic review and economic evaluation. *Health Technology Assessment*, 15(4), 2011.

[72] Van Herk, M., Witte, M., Van Der Geer, J., Schneider, C., and Lebesque, J. V. Biologic and physical fractionation effects of random geometric errors. *International Journal of Radiation Oncology Biology Physics*, 57(5):1460–1471, 2003.

[73] Beltran, C., Krasin, M. J., and Merchant, T. E. Inter- and intrafractional positional uncertainties in pediatric radiotherapy patients with brain and head and neck tumors. *Int J Radiation Oncology Biol Phys*, 79(4):1266–1274, 2011.

[74] Litzenberg, D. W., Balter, J. M., Hadley, S. W., et al. Influence of intrafraction motion on margins for prostate radiotherapy. *International Journal of Radiation Oncology Biology Physics*, 65(2):548–553, 2006.

[75] Bol, G. H., Lagendijk, J. J. W., and Raaymakers, B. W. Virtual couch shift (VCS): accounting for patient translation and rotation by online IMRT re-optimization. *Physics in medicine and biology*, 58(9):2989–3000, 2013.

[76] Kontaxis, C., Bol, G. H., Lagendijk, J. J. W., and Raaymakers, B. W. A new methodology for inter- and intrafraction plan adaptation for the MR-linac. *Physics in Medicine and Biology*, 60(19):7485–7497, 2015.

[77] Kontaxis, C., Bol, G. H., Stemkens, B., et al. Towards fast online intrafraction replanning for free-breathing stereotactic body radiation therapy with the MR-linac. *Phys Med Biol [submitted manuscript]*, 2017.

[78] Köhler, M., Vaara, T., Van Grootel, M., Hoogeveen, R., Kemppainen, R., and Renisch, S. MR-only simulation for radiotherapy planning treatment planning. White paper: Philips MRCAT for prostate dose calculations using only MRI data, 2015.

[79] Edmund, J. M. and Nyholm, T. A review of substitute CT generation for MRI-only radiation therapy. *Radiation Oncology*, 12:28, 2017.

A | Appendix

Displacements between centres of gravity in all three dimensions for each patient separate are shown in Figure A.1. The combined data of this figure was shown before in Figure 3.4. In the histograms is per patient and registration box visible in which direction displacements are most skewed. A skewed histogram could indicate independent motion of LNs in that direction relative to the structures inside the registration box.

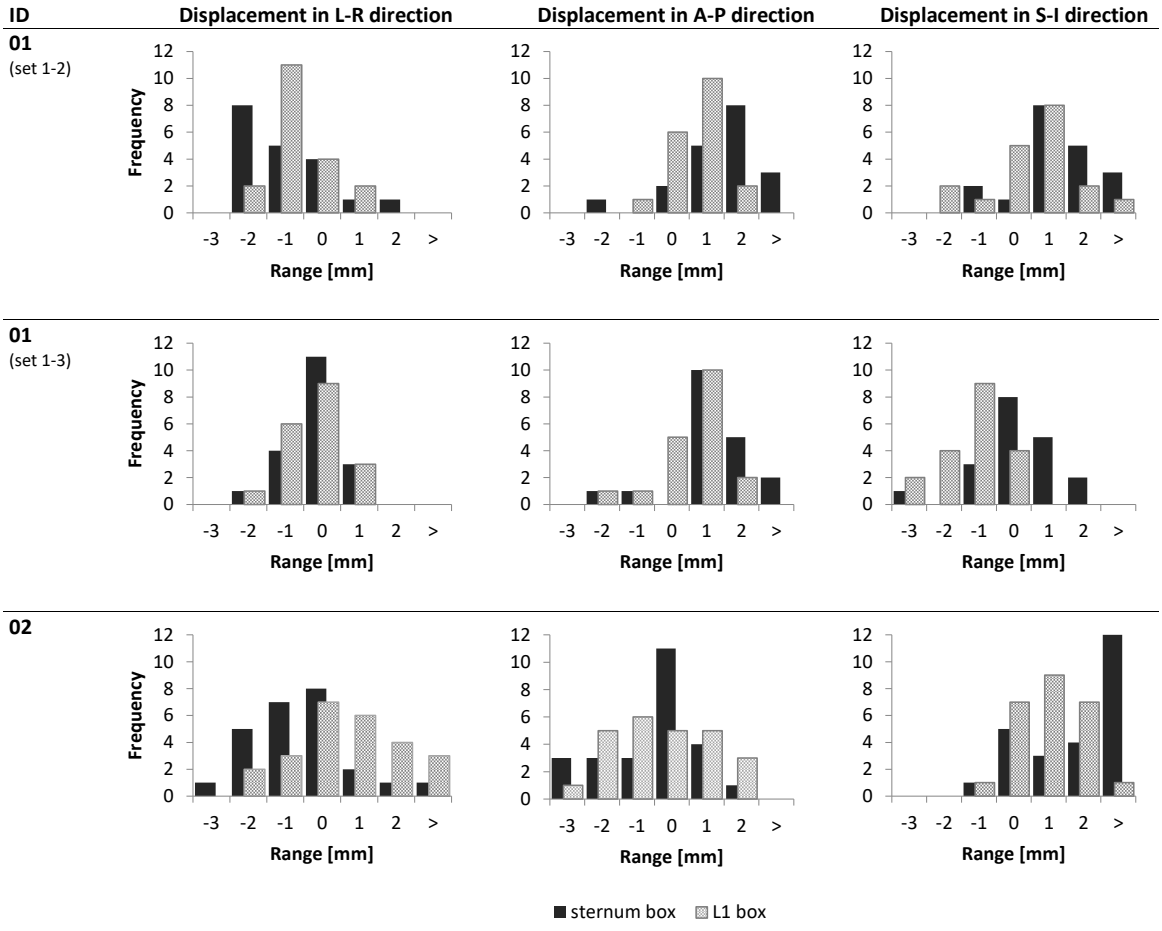

Figure A.1: ***Histograms showing the distribution of centre of gravity displacement for all patients.*** *Displacements for both registration boxes are shown. The x-axis shows the displacement range [mm] and the y-axis shows the frequency of the displacements. Notice the different frequency axes per patient.*

Abbreviations: L: left, R: right, A: anterior, P: posterior, S: superior, I: inferior.

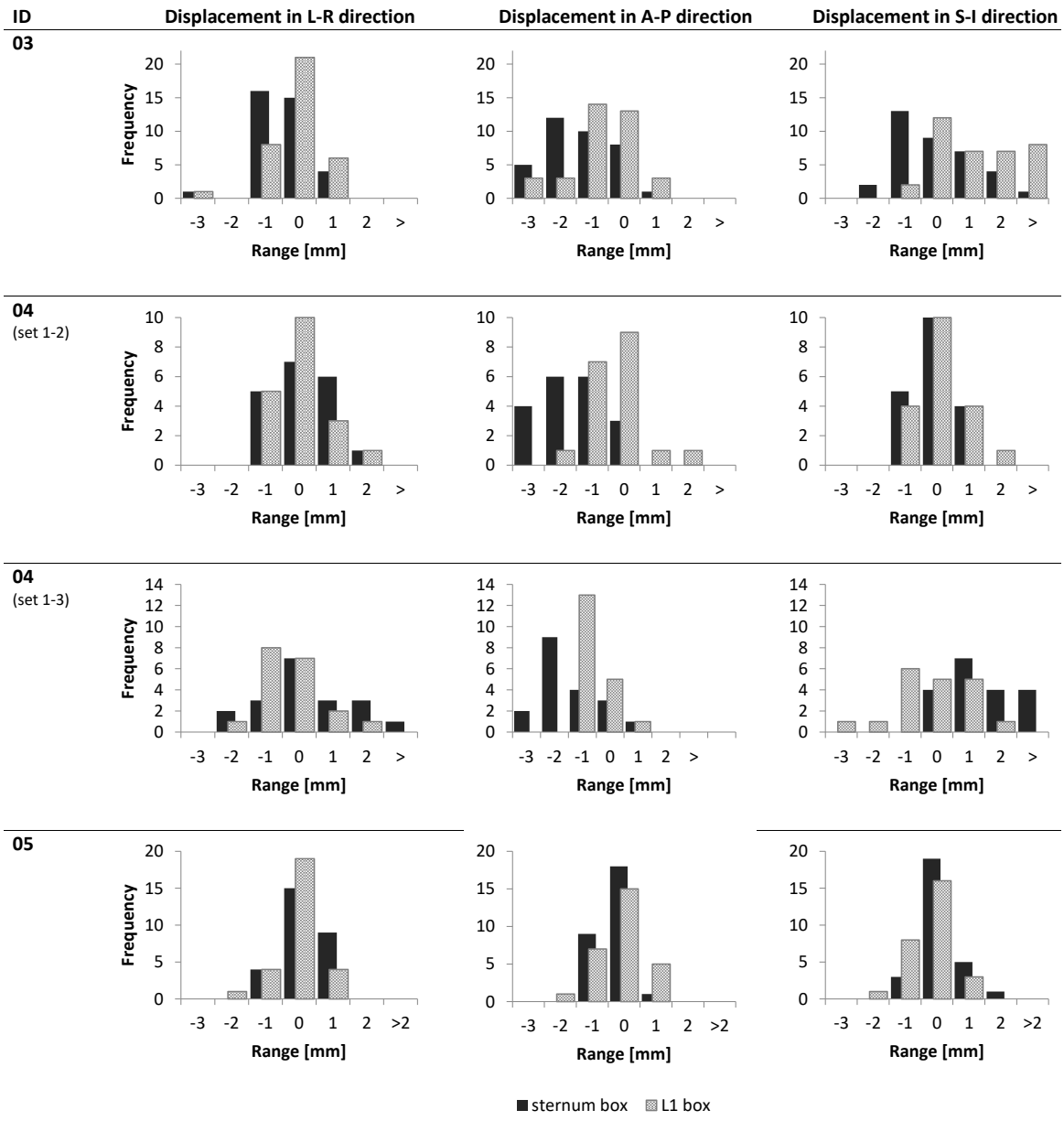

Figure A.1 (continued)

Abbreviations: L: left, R: right, A: anterior, P: posterior, S: superior, I: inferior.